



OPEN Performance and emission prediction using ANN (artificial neural network) on H₂-assisted Garcinia gummi-gutta biofuel doped with nano additives

Harish Venu^{1,2,15}, Manzoore Elahi M. Soudagar^{3,4,5}✉, Tiong Sieh Kiong¹, N. M. Razali^{1,6}, Hua-Rong Wei⁷, T. M. Yunus Khan⁸, Naif Almakayee⁹, M. A. Kalam¹⁰ & Erdem Cuce^{11,12,13,14}✉

The current work focuses on utilization of ANN (artificial neural network) for the prediction of performance and tailpipe emissions of Garcinia gummigutta methyl ester (GGME) enriched with H₂ and TiO₂ nano additives. For experimentation, H₂ gas was introduced to the mixes containing TiO₂ nanoparticles. Diesel, B10 blend (10% GGME biofuel + 90% Diesel), B20 (20% GGME biofuel + 80% Diesel), Diesel-TiO₂ (Mineral Diesel with 100 ppm TiO₂ nano additives), B10-H₂-TiO₂ (B10 blend with 100 ppm nano additives + 5 L/min of H₂) and B20-H₂-TiO₂ (B20 blend with 100 ppm nanoparticles + 5 L/min of H₂) were considered for experimentation. A constant mass flow rate of 10 L/min was used for the hydrogen flow throughout the test procedures. Test results were carefully analyzed to determine the performance and emission measures. Different speeds between 1800 and 2800 rpm were used for each test. When combined with pure Diesel and mixtures of biodiesel, these nanoparticles and hydrogen enhanced the performance data. For instance, the brake-specific fuel consumption was reduced but the power, torque, and thermal efficiency were increased. Although there was a modest rise in NO emissions, the primary goal of lowering CO, CO₂, and other UHC emissions was met. The ANN models confirm and agreed the Diesel engine experimental work possesses minimal root mean square error (RMSE) and correlation coefficient values were estimated. This ideal model predicts and optimizes the engine output at a higher accuracy level, which gives better results compared with other empirical and theoretical models.

Keywords Artificial neural network, Garcinia gummi-gutta biodiesel, Diesel engine, Performance and pollutant emissions

¹Institute of Sustainable Energy, Universiti Tenaga Nasional, Jalan IKRAM-UNITEN, 43000 Kajang, Selangor, Malaysia. ²Centre of Research Impact and Outcome, Chitkara University, Rajpura, Punjab 140417, India. ³College of Engineering, Lishui University, Lishui 323000, Zhejiang, China. ⁴Chitkara Centre for Research and Development, Chitkara University, Baddi, Himachal Pradesh 174103, India. ⁵Division of Research and Development, Lovely Professional University, Phagwara, Punjab, India. ⁶AAIBE Chair of Renewable Energy, Universiti Tenaga Nasional, Jalan IKRAM-UNITEN, 43000 Kajang, Selangor, Malaysia. ⁷Department of Photoelectric Engineering, Lishui University, Lishui 323000, China. ⁸Department of Mechanical Engineering, College of Engineering, King Khalid University, 61421 Abha, Saudi Arabia. ⁹Department of Industrial Engineering, King Khalid University, 61421 Abha, Saudi Arabia. ¹⁰School of Civil and Environmental Engineering, FEIT, University of Technology Sydney, 11, Ultimo, NSW 2007, Australia. ¹¹Department of Mechanical Engineering, Faculty of Engineering and Architecture, Recep Tayyip Erdogan University, Zihni Derin Campus, 53100 Rize, Turkey. ¹²University Centre for Research and Development, Chandigarh University, Mohali, Punjab 140413, India. ¹³Department of Mechanical Engineering, Saveetha School of Engineering, Saveetha Institute of Medical and Technical Sciences, Saveetha University, Chennai, India. ¹⁴Center for Research Impact & Outcome, Chitkara University, Rajpura, Punjab 140401, India. ¹⁵Department of Condensed Matter Physics, Saveetha school of engineering, SIMATS, Chennai, India. ✉email: manzoore@lsu.edu.cn; erdem.cuce@erdogan.edu.tr

Abbreviations

ACO	Ant Colony Optimization algorithm
ANN	Artificial neural network
ASTM	American Society for Testing and Materials
B10	10% raw Garcinia biodiesel + 90% petroleum-diesel
B10-H ₂ -TiO ₂	B10 blend + 50 ppm TiO ₂ nano particles + 10 ppm H ₂
B20	20% raw Garcinia biodiesel + 80% petroleum-diesel
B20-H ₂ -TiO ₂	B20 blend + 50 ppm TiO ₂ nano particles + 10 ppm H ₂
BP	Brake power
BSFC	Brake specific fuel consumption
BTE	Brake thermal efficiency
CI	Compression ignition
CO	Carbon monoxide
CO ₂	Carbon dioxide
DEE	Die-ethyl ether
DI	Direct ignition
Diesel-TiO ₂	100% diesel + 50 ppm TiO ₂ nano particles
EGT	Exhaust gas temperature
EN 14214	European Committee for Standardization
FAME GO	Fatty acid methyl ester of garcinia oil
FCC	Face Centred cubic
Fe ₃ O ₄	Iron oxide
FT-IR	Fourier-transform infrared spectroscopy
GA	Genetic algorithm
GC-MS	Gas chromatography-mass spectrometry
GGME	Garcinia gummi-gutta methyl ester
HC	Hydrocarbon
HRR	Heat release rate
HSU	Hartridge smoke unit
IC	Internal combustion
ID	Ignition delay
IOMNP	Iron oxide magnetic nano particle
kW	KiloWatt
LM	Levenberg Marquardt
MLP	Multilayer perception network
NOx	Oxide of nitrogen
O ₂	Oxygen
R	Regression coefficient
R ²	Determination coefficient
SEM	Scanning electron microscope
TEM	Transmission electron microscope
TL	Thermomyces lanuginosus
UBHC	Un-burnt hydrocarbon
VCR	Variable compression ratio
XRD	X-ray diffraction

The use of the previous global energy drive summary indicated that the primary source of energy utilised stems from the internal combustion (IC) engines' igniting of petroleum-based fuels. According to current estimates, the world's recoverable stocks of petrol and petroleum are expected to reach 7.289 trillion cubic feet and 1.44 trillion barrels, respectively, based on the global energy scenario¹. A total of 261 billion cubic feet of petrol and 86.5 million barrels of oil are consumed daily by people worldwide. Global oil and natural gas reserves were depleted in 40 and 60 years, respectively, due to recent consumption patterns². Because of their inherent physiochemical and oxidation components, hydrocarbonated and liquidity fuels consume a significant portion of the market. Unfortunately, the capitals of non-renewable energy fuels have declined, thus it may remain empty for a few decades.

Figure 1 shows that, as of 2019², Asia is the continent that consumes the most oil, hydropower, lignite, and coke on a global scale. In the field of electricity generation, Europe and Eurasia are the biggest users of nuclear power, petrol fuel, and renewable resources. In terms of worldwide coal consumption rate, accounting for three-quarters of global energy consumption, the Asian continent holds the top spot among all users. In every sector, the energy consumption ratios in the Middle East and Africa were negligible, whereas North America's energy consumption rate is moderate. In the years that followed, the universal oil consumption rate climbed gradually (Fig. 2).

The alarming impacts of global warming are attributed to a number of sources, including hazardous waste produced by companies, toxic goods derived from petroleum products, and some chemical items. This will be the main cause of rising food prices, changing climatic patterns, and threats to the survival of humanity. In the next 25 years, India hopes to achieve the sustainable evolution rate of 8.5–10% in the economic sector, in order to maintain the people's living standards and further personal growth events. In the future, it will be possible to increase the major energy band supply by 4–5%. Regaining the nation's future energy demands may depend on

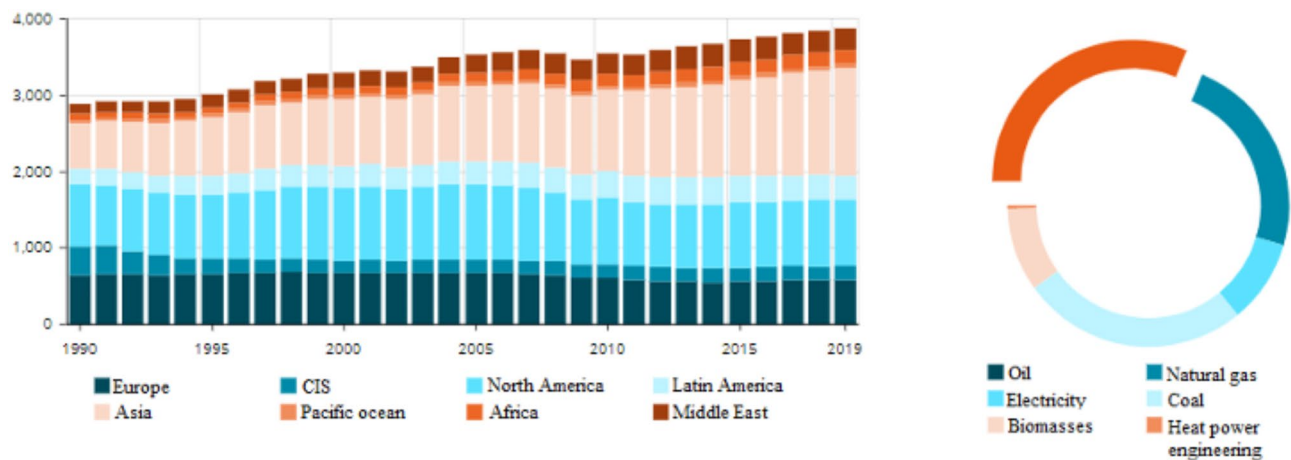


Fig. 1. Fuel consumption rate by various continents (Data sourced from²).

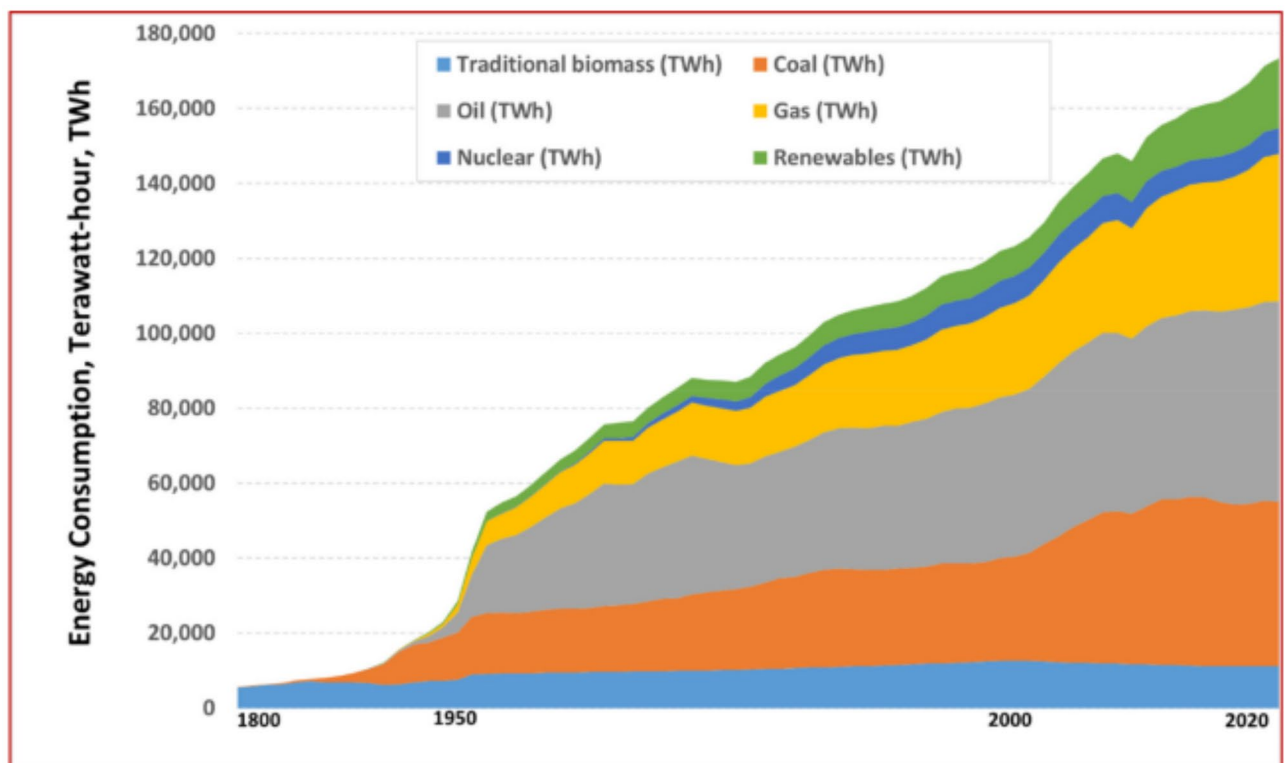


Fig. 2. Global energy consumption by various sectors (Data from³, available online: <https://ourworldindata.org/energy-productionconsumption>).

striking a balance between the energy crisis and the upcoming investigation of alternative fuel energy sources with low emission levels.

Due to the lack of conservative fossil fuels, the increase in fuel prices, and the multiplied emissions of toxins produced during the oxidation process, biodiesel and biofuel sources have proven to be highly amazing in the current decades. The deposits of petroleum oil and its byproducts are concentrated in a few isolated areas around the country, and they regularly run out. The likelihood of producing biomass and biodiesel from locally grown sources and using them to replace different petroleum-based commodities is the most appealing way to overcome the fuel energy deficit. Biodiesel and biomass sources are advantageous renewable fuels that are generated through natural processes such as aero-biotic or agricultural digestion, as opposed to the geological delivery method used to manufacture raw crude oils like lignite, coke, and crude oil⁴.

In their study, Kasiraman et al.⁵ examined the effects of using cashew nut methyl ester, raw cashew nut oil, and various combinations of vegetable oil, oxygenating additives, and alcohols on the performance of the CI

engine. The authors concluded from their observations that, of the different oxygenate additives, Die-ethyl ether 30% (DEE) evolved to have a more excellent Brake Thermal Efficiency (BTE) of approximately 29.68% at peak load conditions. Additionally, the authors found that tailpipe emissions, including nitrogen oxide (NOx) and smoke opacity, also showed better results in comparison to other additives. When compared to other alcohol additive mixes, butanol (butanol 30%) has superior fuel economy, BTE, and Heat Release Rate (HRR). Then, on a volume basis, the analysis was expanded to include several vegetable oil blends and cashew nut methyl ester. Among these, blends of camphor oil (CMPRO30) showed the highest levels of thermal efficiency, HRR rate, NOx, and smoke opacity. Using three different *Pistacia lentiscus* biodiesel ratios with diesel—5%, 30%, and 50% by volume basis—Khiari et al.⁶ studied the naturally occurring CI engine. According to the author's observations, *Pistacia lentiscus* biodiesel has a roughly 3% increase in thermal efficiency when compared to hydrocarbon fuel. It also significantly reduces tailpipe emissions of unburned hydrocarbon fuel, carbon, and particulate matter at 100% load condition—roughly 45%, 25%, and 17%, respectively. Higher levels of BSFC (Brake Specific fuel consumption, which is a measurement of how much fuel an engine consumes in relation to the power it produces) and NOx are also found—about 10% and 4%, respectively.

A diesel engine running on petroleum-diesel mixes and fuelled by *Ceiba pentandra* and *Jatropha curcas* biodiesel had its performance and exhaust emissions examined by Dharma et al.⁷. More engine torque can be achieved using B10's CI engine performance, which is generally comparable to that of petroleum-Diesel fuel; different mixes were shown to correspond with varied levels of brake power (BP) and brake torque (BTE). When 50% *Jatropha curcas* and 50% *Ceiba pentandra* biodiesel are blended with hydrocarbon fuel, the amount of CO and smoke opacity emissions are reduced; however, nitrogen oxide and CO emissions are increased simultaneously. The test engine exhaust emissions and performance metrics were also predicted using ANN models, which produced outstanding results with a coefficient of determination of greater than 98% and a mean absolute percentage error of less than 5% for all parameters. An explicit mathematical representation is typically not necessary for ANN models to produce accurate and trustworthy results. In order to predict the engine exhaust emission and performance parameters of the CI engine operating in dual fuel mode using hydrogen gas and *Jatropha* biodiesel, Javed et al.⁸ investigate the application of the ANN model. The ANN tool was developed to estimate engine performance and emissions, such as NO, CO, O₂, HC, CO₂, and EGT, by adjusting load, hydrogen flow rate, and biodiesel blends. Regarding this, the suggested ANN tool's gross regression coefficient, mean square error, and mean absolute percentage error are, respectively, 0.9936, 0.0011, and 4.86%.

The integration of ANN with Ant Colony Optimisation (ACO) algorithm was handled by Mohammadhassani et al.⁹. The relationship between input parameters was illustrated using the feed-forward multilayer perceptron network and the multilayer perceptron (MLP) network. With pertinent correlation factors of 0.96 and 0.98, ANN suggests the appropriate soot and NOx model. The ACO algorithm was developed to determine the ideal temperature for engine air consumption and injection fuel at varying power and speed levels, taking into account engines with significantly reduced emissions of NOx and soot. In comparison to the combination of Genetic Algorithm (GA) and ANN, the convergence speed of the ACO and ANN tools was comparatively more significant. The ANN modelling technique in this investigation primarily estimated tailpipe emissions levels at the lowest possible time and produced a higher anticipated rate with greater accuracy. The author proposes using this modelling technique to lower soot and NOx emissions in the electronic control unit industry.

The ANN tool was used to forecast the CI engine's output when Ude et al.¹⁰ studied the engine's performance using cottonseed biodiesel. Petroleum-Diesel, biodiesel, and their blends are used in experimental testing in a two-cylinder DI Diesel engine to achieve varying engine speeds. Raw cottonseed oil and mineral diesel test fuel mixes were used to experiment with CI engines, and the results showed better performance levels with low emissions. When comparing raw petroleum-diesel fuel outcomes, such as BP, BTE, BSFC, minimum CO, and HC emissions, B20 blend has produced results that are comparable. The ANN tool, which finds the R-correlation coefficient by 0.9743, 0.9914, and 0.9788, optimised and predicted the experimental data, such as BP, BTE, and BSFC, in the interim. Furthermore, the model illustrates the range of 0.0001 for the mean square error between the simulated and measured output. In conclusion, the engine efficiency of the biodiesel mix derived from cottonseed oil is improved, and the engine parameter is accurately predicted by the ANN tool. The quality of biofuel is expected to significantly improve with the addition of hydrogen flow. Hydrogen gas is needed in many industries, such as the transportation, fertilizer, and petroleum refining sectors. Hydrogen is an environmentally friendly fuel that may be produced using nuclear power, natural gas, biomass, and sustainable energy sources including solar and wind power. Hydrogen is an energy carrier that improves the performance of the primary fuel.

Nano additives play a major role in lowering the exhaust emissions from diesel engine. Several researches were done on nano additives which are metal oxide based additives which can liberate oxygen during combustion and thereby oxidize the unburnt hydrocarbons and carbon monoxide to carbon dioxide and water vapour. Table 1 shows the literatures used with different nano particles and their effect in base fuel in enhancing the characteristics.

According to the literature review mentioned above, diesel engines are thought to produce more harmful pollutants since they use fossil fuels, and there will be a greater need for this kind of energy in the near future. The world's fuel and food crises are lessened, and pollution of the land, water, and atmosphere is reduced thanks to the innovative lipase immobilisednanocatalystutilised to produce *Garciniabiodiesel* from inedible *Garcinia* seeds¹¹. Due to the low percentage of biodiesel produced using standard methods, a lipase immobilisednanocatalyst was employed to increase the total yield of *Garcinia* biodiesel, which met the requirements to be utilised as a substitute fuel for diesel engines. Next, different test fuel blends made from the *Garcinia* biodiesel were created, and the fuel's characteristics regarding pollutant emissions and engine performance were examined using a diesel engine. Next, using the ANN modelling tool, the diesel engine properties of *Garciniabiodiesel* and its fuel mixtures were anticipated and optimised. Research on the expected and optimised properties of the innovative

Researcher	Nano additive and surfactant concentration	Base fuel and surfactant	Engine specification	Significance
Sivakumar et al. ⁶⁸	Al ₂ O ₃ (50–100 ppm), Cetyltrimethylammonium bromide	Palm oil methyl ester	Single cylinder, 4 S, Kirloskar AV1, 210 bar IP and 23degBTDC IT, 16.5:1 CR, 1500 rpm	7% high BTE, lowered BSFC, HC, CO, higher NOx emissions
Ranjan et al. ⁶⁹	MgO (30 ppm), 4-Chlorobenzoyl chloride	Waste cooking oil biodiesel	Single cylinder, Kirloskar TV1, vertical, 1500 rpm, 17:1 CR, load (4.7–18.11 kg)	Higher BP, BSFC and BTE, CO ₂ , Lowered HC, CO and NOx, Improved combustion
Mehregan et al. ⁷⁰	Manganese oxide and cobalt oxide (25 ppm and 50 ppm), no surfactant	B20 waste frying oil	4 Cylinder, 4Stroke Urea-SCR Direct Injection, CR 17.9: 1, IP210 bar, IT 23 deg bTDC	Lowered SFC at part and full load, higher thermal η , drastic reduction of NOx and CO
El-Seesy et al. ⁷¹	Al ₂ O ₃ (50–100 ppm), 20 mg per lit., no surfactant	Jobba oil methyl ester	Deutz F11511, 1 cyl, 4 S, DI, 1500 rpm, IP175 bar, IT 24 deg bTDC	NOx 70%↓, CO 80%↓, HC 60%↓, and Smoke 35%↓, 12% drop in BSFC
Hoseini et al. ⁷²	Graphene oxide (30,60 and 90ppm), no surfactant	Ailanthus altissima biodiesel	Lombardini Diesel3LD510, 1800 rpm, 17.9:1 CR, 1 cyl, non-turbocharged, 32.8Nm torque	↓HC, ↓CO, ↓BSFC, ↑NO _x and ↑CO
Kumar et al. ⁷³	Ferrous oxide and ferrofluid (0.5%, 1% and 1.5%), surfactant: 2 mol of NaOH	B20 palm oil methyl ester	Single cylinder, 4 S, Kirloskar TV1, 210 bar IP and 23degBTDC IT, 16.5:1 CR, 1500 rpm	↑ BTE (by 16.6%), ↓BSFC (by 11.1%), other emissions reduced simultaneously
Ashok et al. ⁷⁴	Zinc oxide (50 and 100ppm), Ethanox (200 and 500 ppm) Surfactant: Alcohol	CalophyllumInophyllum methyl ester	Simpson S217, Two cyl 4 S, DI, Vertical, IT 23 deg bTDC, IP 200 bar 18.5:1 CR	High BTE for ZnO (29.5%) than Ethanox (26.8%), lowest BSFC for ZnO50 ppm, 18.4% and 13% less CO and HC for ZnO 50 ppm, 17.8% less NOx for Ethanox (500 ppm), 12.6% less NOx for ZnO100 ppm.
Leo et al. ⁷⁵	Al ₂ O ₃ and FeCl ₃ (50 and 100 ppm), no surfactant	Waste cooking oil biodiesel (WCOB)	Homogeneous CCI-DI, 210 bar IP and 23degBTDC IT, 17.5:1 CR, 1500 rpm, 4.4 kW	HC reduced by 54.17%, NOx reduced by 4.3%, 100ppm additive lowers 30.4% smoke in diesel, 23.65% in WCOB
Mohanraju et al. ⁷⁶	Aluminium nitrate (Al (NO ₃) ₃) nanoparticles and graphene oxide nanoplates (GONP _s) 50 ppm, no surfactant	Industrial leather waste fat biodiesel	Single cylinder, Kirloskar TV1, vertical, 1500 rpm, 17:1 CR, load (4.7–18.11 kg)	CO ₂ ↓6.84%, HC↓13.11%, and smoke ↓5.75 emissions for Al (NO ₃) ₃ nano particles
Jayabal et al. ⁷⁷	Bio-silica (Bio-Si) 50-100 ppm, no surfactant	Leather waste fat biodiesel	Kirloskar TV1, vertical, 1500 rpm, 17:1 CR, 210 bar IP and 23degBTDC IT	Higher BTE and lowered NOx for 50 ppm additive fuel. For 100ppm additive, HC and CO reduced by 31.87% and 34.14%, but NOx increased by 4.45%.

Table 1. Overview of a variety of nano additives and their influence on characteristics of engine.

Garcinia seed biodiesel and its engine characteristics is carried out in the research community using the ANN modelling tool. This study was completed using waste Garcinia seed biodiesel that was trans-esterified using a lipase immobilised nanocatalyst. The biodiesel was then synthesised and characterised using TEM, XRD, and SEM instruments, yielding a yield of over 92% biodiesel. The fuel blends were then prepared using a magnetic stirrer method and analysed using FT-IR and GC-MS instruments. To reduce the need for and demand for fossil fuels, the Garciniabiodiesel and its fuel mixes were tested in a single-cylinder diesel engine. The ANN modelling tool was then used to forecast and optimise the engine's characteristics.

Materials and methods

Novel nanocatalyst preparation, *Garcinia* oil and biodiesel production

Novel nanocatalyst preparation and its technique

Nowadays, there are a lot of active applications using nanotechnology and related nanomaterials. As a result, nanostructured additives are used to immobilise the well-known biocatalyst. In this study, the chemical binding of Fe₃O₄ magnetic nanoparticles, which acted as a core and an enzyme as a shell to create core-shell nanoparticles, successfully completed the immobilisation process. *Thermomyceslanuginosus* lipase (TL) was positively immobilised in conjunction with the Fe₃O₄ magnetic nanoparticle for this reaction by means of a co-precipitated approach. This collection of reactions is described as an innovative technique using lipase-immobilized Fe₃O₄ magnetic nanoparticles.

The co-precipitation method was first used to create iron oxide nanoparticles. Ammonia solution was added after ferric and ferrous chlorides were mixed at a molar ratio of 2:1, reserved in 0.2 mol, and dissolved in 200 millilitres of distilled water for this synthesis. The pH of 9 was achieved by including this solution, and a mechanical stirrer was used to mix it often. Following a 12-h ageing period, the necessary Iron Oxide Magnetic Nano Particle (IOMNP) material was obtained. To remove any contaminants from the obtained solution, the produced IOMNPs were then separated using the centrifugation technique. Three or four times, it was cleaned using ethanol and acetone. After removing the moisture content, the produced nanoparticles were vacuum-sealed at 60 °C for 11 to 12 h, and the IOMNP were stored in airtight bottles.

Previous research by Subramani et al.⁵⁰ was cited as the source of the overall process for immobilising lipase enzyme within IOMNP. The carbodiimide activation procedure achieved the covalent connection of *Thermomyceslanuginosus* (TL) lipase immobilisation with IOMNP, as was previously discussed. In relation to this, IOMNP were permitted to suspend in 0.2 mol of NaCl and 0.005 mol of phosphate buffer at eight pH. After 0.6 ml of 0.04 g/ml carbodiimide solution mixed with phosphate buffer at room temperature, it is combined for 20 min of sonification process. The carbodiimide agent and TL were mixed repeatedly after being left in the stirrer for 40 min at 5 degrees Celsius. With IOMNP attributable to its magnetic nature, the TL was effectively immobilised now. The external magnetic field separated it, and it was then recycled for the subsequent batch operation, which is illustrated in Fig. 3. Finally, immobilised IOMNP was placed in storage to be examined later.

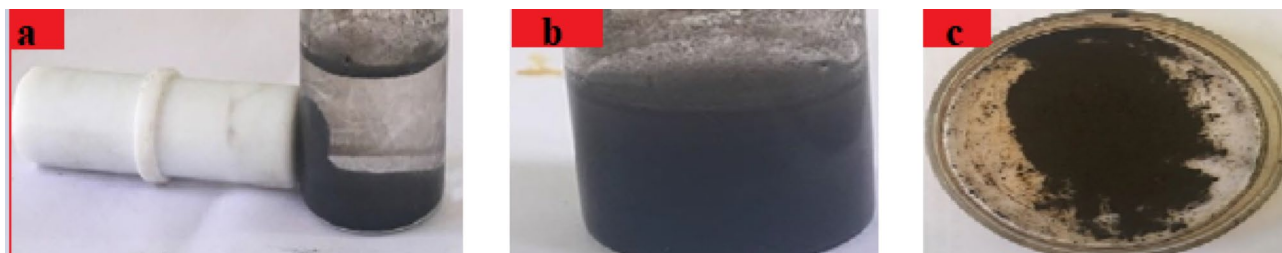


Fig. 3. (a) Immobilized Fe_3O_4 nanoadditives separated by the external magnet. (b) Synthesized Fe_3O_4 nanoadditives (c) dried Fe_3O_4 nanoadditives.



Fig. 4. Oil extraction process of raw Garcinia oil from *Garcinia* seed.

After using the supernatant approach, the Bradford process was used to obtain the lipase enzyme. Removing the excessive immobilised lipase from the net assessed amount of lipase for the immobilisation process allowed for the regular determination of the immobilised lipase quantity. Equation (1) below was used to determine how well immobilised lipase reacted to form magnetic nanoparticles.

$$I = \frac{(\text{CO}_i - \text{CO}_f)L_1}{\text{CO}_i L_2} \quad (1)$$

Herein, I is the Immobilization efficiency (%), L_1 and L_2 is the volume of solution in cm^3 , CO_i and CO_f is the initial and final lipase concentration rate in the supernatant.

Garcinia seed oil extraction and its preparation approaches

Garcinia seeds are mostly obtained from the National Bureau of Plant Genetic Resource (NBPGR) located in the Kerala, India, Thrissur region. After the seeds were sorted according to size and shape, they were dried for two to five days to remove any remaining moisture, and then they were roasted for twelve hours at 101°C . The grinder is then used to grind the available seeds into a fine powder, and the traditional mechanical expeller process is used to extract the raw *Garcinia* seed oil from the powdered seeds. With 1 kg of *Garcinia* seed supply, this approach yields a greater level of 40%. The resultant consequence ought to surpass the results of the solvent extraction technique. Yet, due to its higher inherent oil content than other conventional seed sources, *Garcinia* seed oil can provide higher output levels at the mechanical extraction stage itself (Yatish et al., 2018). Using European and ASTM standards as a basis, the desirable fuel qualities were measured and examined. Figure 4 shows the flow of the *Garcinia* seed oil process. The following Eq. (2) was used to predict the raw *Garcinia* oil yield:

$$\text{Total Weight of Oil Yield (\%)} = \frac{\text{Weight of Extracted Oil (g)}}{\text{Weight of } \textit{Garcinia} \text{ Seeds (g)}} \times 100\% \quad (2)$$

*Lipase immobilized with Fe_3O_4 catalyst transesterification process of *Garcinia gummi-gutta* seed oil*

As was previously mentioned, this process involved the careful selection and use of a unique lipase immobilised transesterification activity to achieve an exceptional yield and improved biodiesel quality. Initial steps of this technique included TL immobilised Fe_3O_4 nanoparticles (1–6%), raw *Garcinia* fuel (1 L), and methanol (2–14%). The enhanced reaction temperature (20–70 °C) and time (12–74 min) were used for this study.

Previous study findings^{12–15} were used to determine these ideal settings for this lipase-based transesterification procedure. From the Nanoscience Laboratory at the AC Tech Campus of Anna University in Chennai, the lipase-based transesterification reaction was carried out. The laboratory also handled the raw ingredients, glassware, and other equipment. The initial transesterification activity using a 500 ml airtight empty bottle and a lipase immobilised catalyst (Fe_3O_4 + *Thermomyceslanuginosus*) was conducted. 250 ml of raw *Garcinia* oil and 1% of immobilised Fe_3O_4 were then added to the bottle, which was closed and divided. The mixture was then manually swirled to combine the ingredients. With pellets in the arrangement, it was placed in a magnetic stirrer, and 800–1000 rpm stirring was used to achieve the desired operating condition. A magnetic stirrer is often used to initiate the reaction at 20 °C for 12 min. Lipase immobilised transesterification starts under ideal working circumstances when the filled airtight bottle is stirred magnetically.

Fatty Acid Methyl Ester of *Garcinia* Oil (FAME GO) and glycerol are produced when the immobilised lipase enzyme (TL) breaks down all of the triglycerides in the raw *Garcinia* oil at the conclusion of the stirring process. Additionally, to overcome the excess biodiesel yield, the immobilised lipase enzyme drives the reaction and aids in converting the raw *Garcinia* oil's highest ratio of triglycerides.⁷ After stopping the lipase-based reaction, the natural reaction mixtures were added to the separating funnel arrangement, which allowed them to remain in a cool, balanced environment. With a higher yield of production rate, the FAME GO was extracted straight from raw *Garcinia* seed oil following the completion of the separation process, stimulated by lipase immobilised catalyst. The extractable FAME GO was gathered in the beaker that was left empty, and the glycerol content was separated. Figure 5 illustrates the lipase immobilised transesterification development. Following this, the FAME GO (reaction mixture) was heated to a maximum of 40 °C in order to remove the biodiesel's accessible contaminants as well as its greater water and methanol content. Several sets of the batch method of producing *Garcinia* biodiesel were used to continue this same process.

The best conditions for FAME GO conversion were found to be reaction temperature (40 °C), catalyst immobilisation (5% w/w), reaction duration (62–74 min), and methanol (6%) with the highest average biodiesel percentage of 92.12 yielded as a result of these factors. This evaluation was based on the results of all batch processes. Due to a higher reaction rate and greater biodiesel output, methanol content was added to the reaction mixture three times in this case. FAME GO (biodiesel) was found to be highly miscible with petroleum diesel when the mixture was centrifuged for 12 to 15 min. When biodiesel was combined with raw diesel, various miscibility ratios were tested; no changes were seen after 15–20 days.

With the assistance of the external magnetic field, immobilised lipase was finally removed from the mixture and cleaned with distilled water and alcohol to get rid of any undesired contaminants. For the following batch process, it was then frozen and kept intact. Utilising the biodiesel reactor's higher capacity for this reaction under optimal conditions allowed for the bulk synthesis of FAME GO (biodiesel). Instruments from FT-IR and GC-MS were used to diagnose the acquired FAME GO.

*Assessment of raw *Garcinia* biodiesel properties compared with petroleum-diesel fuel*

Since *Garcinia gummi-gutta* seed oil has unfavourable fuel qualities and satisfies both ASTM D6751 and EN 14214 standards, it was selected as the innovative alternative feedstock for this experimental study project. Raw

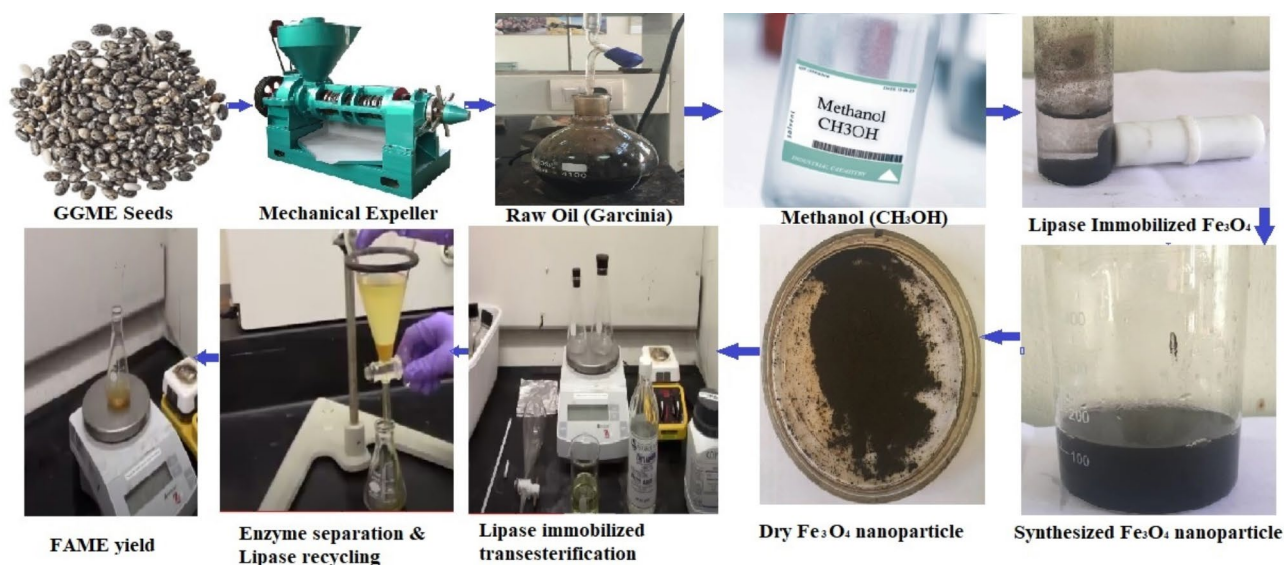


Fig. 5. Integrated process flow of *Garcinia* Biodiesel production with lipase immobilized nanocatalyst.

Garcinia oil also satisfies ordinary petroleum diesel requirements. The lipase immobilised catalyst achieves the best biodiesel output while also contributing to the reduction of environmental contaminants. This generates an environmentally benign natural energy fuel for human use. The attributes of unrefined GGME blends with petroleum-based diesel are explained in the description that follows. The characteristics of raw Garcinia and Jatropha biodiesel were then contrasted. The lab was used to measure and estimate all pertinent parameters. Table 2 compares the fuel characteristics of Garcinia biodiesel and its blend.

ANN modelling and its approach

- The most advanced ANN technique is part of an experimental data-processing toolkit developed by biological neural networks, and it shares some performance and technical characteristics with them. The main use for this ANN model is to analyse non-linear problems using an experimental and dependable method in order to test, train, and target the forecast of various parameters, such as engine performance and tailpipe emissions of GGME and its blends with petroleum-Diesel. The R-regression coefficient and relativity errors of the input data were obtained by running this ANN model. The GGME Biodiesel engine's efficiency and tailpipe emissions were then predicted and optimised by the model.
- ANN modeling and its organization.

The current study used the MATLAB software platform to build an artificial neural network (ANN) model and program to forecast and analyse the BTE, BSEC, HC, CO, CO₂, NO_x, and smoke opacity of GGME blends mineral diesel of experimental engine output. The learning method known as LM, or Levenberg Marquardt, was also utilised to run this ANN model. ANN network architectures are created using this algorithm between^{16,19}. Parallel to this, it was demonstrated that the LM method was a learning algorithm that performed expertly, built the network fairly, and was referred to as having an excellent network structure in ANN modelling with rapid data processing. To guide simulation and forecast of GGME and its mixtures' performance and emission, this learning method was put into practice. A target data set was constructed at the time of model execution using 30% of the engine experimental data that was framed for this modelling, with the remaining 70% of the data being assigned for testing and training purposes^{17,18,20,21}. With values of 0 s and 1 s, the task was carried out by the famed logistic sigmoid transfer function, which was coupled in this ANN model. Primarily, input and output dataset normalisation was completed previously.

From 10 to 19, neurones were initiated in the system, which was run with two sets of inputs (Blend and Brake power). ANN's input, hidden, and output layers—all produced by a group of nodes—are its primary processing steps. Projected to the hidden layer are artificial neurones that process input data obtained from experimental engine tests. When processing took place in the hidden layer, data from ANN neurones that were accessible in the input layer helped to record the pertinent output. The desired output was sent to the output layer once the hidden layer satisfied its goals of screening and prediction. The system calculates the weighted sum values and can be used to instigate the system summation function to fix the net input transformed into the cell.

Fuel mixes were the input parameter, and BP may be identified as input data to the cells. With this information, the generated network can train on the inputs. In addition, one can estimate the input data and processing method with its components by accessing weight functions. Each value of input into this system must be multiplied by its weight value. The processing parts are then connected using a summation function grouping scheme. The net information of the network was ascertained following these assessments. This curvilinear approximation of the relationship between the given input and output data was obtained by computing the system activation function. Furthermore, by using the net-input value to the designated cell, the estimated output of the cell was determined. Various functions that have been allowed may have an impact on the activation function's effectiveness. In order to overcome these challenges, the logistic sigmoid transfer function was chosen as an initiating function. This function has several advantages, including the ability to handle non-linear functions and continuous and diverse processes.

The backpropagation method was designated as a general learning algorithm, and a variety of learning algorithms were worked on to improve the weight function in the ANN model. The weight function is updated only by this backpropagation technique in tandem with the variations in the network's output and its data, which was processed to produce the best outcomes⁴⁰. In the artificial neural network model, these machine learning parameters were often constrained and active. Adaptive rule, conjugate gradient, Bayesian regularises, and Levenberg-Marquardt method were the frequently used training functions for the artificial neural network (ANN). The LM method was applied to a hidden layer consisting of numerous neurones that were set up in a network structure for a powerful operation that produced an excellent result and a perfect match between the output values and the experimental test values.

Test fuel properties	Units	Diesel	B10	B20	Garcinia gummi-guttabiodiesel	ASTM D6751	EN 14214
Density @ 15 °C	g/cm ³	0.831	0.834	0.837	0.886	0.858	0.86–0.90
Viscosity @ 40 °C	mm ² /s	3.2	3.6	3.9	5.14	1.9–6.0	3.5–5
Flash point	°C	70	77	86	181	Min.130	Min.120
Cetane number	–	46	48	50	57	Min.47	Min.51
Higher heating value	MJ/kg	43.82	43.02	42.12	39.88	–	Min.35

Table 2. Test fuel properties of *Garcinia* Biodiesel and its blends compared with petroleum-diesel⁵².

- (c) ANN architecture and its network activity.
- (d) Neurons in the hidden layers with a transfer function are followed by neurones trained with layers in the general architecture of artificial neural networks¹⁹. Typically, the output layers of the ANN model were configured with the hidden layers, and the input layer was configured with hidden layers. The suggested study employed a feed-forward neural network criteria, wherein the training set and network underwent continuous modification through successive model iterations contingent on data inputs. Incorporating production and a hidden layer of the ANN model, the output of this network was finally evaluated. The ANN model's output layer and hidden layer were previously assessed, as was the feed-forward network and transfer function. A crucial requirement for networks and network performance simulation, the transfer function selection for this ANN model is required to be included in the learning rule. To evaluate the descriptive response, this model's transfer function was put into practice.

Gradient descent activity gradually dictated the errors of the ANN network through the backpropagation learning technique, which was formerly known as feed-forward architecture. The Levenberg–Marquardt training technique and the back propagation neural network—the artificial neural network architecture shown in Fig. 6—were both selected for the accurate models. Biodiesel is a valuable substitute for traditional fossil fuel, according to Karthickeyan et al.²⁵. The ANN model tool utilised in this work estimates and forecasts performance and emissions using seven different training techniques. Levenberg–Marquardt (trail), which yields log and tan sigmoidal transfer function outputs, is the finest of the seven methods. Using various mixtures of biodiesel, the recommended ANN modelling method predicts engine performance and tailpipe emissions with high accuracy. With petroleum-Diesel at all compression ratios, the fuel mix B20 demonstrated the BTE and decreased the BSFC. Except for NO_x emissions, this fuel blend has substantially lower CO and HC emissions than petroleum-diesel²². Kannan et al. investigates the effects of using Waste Cooking Palm Oil (WCPO) biodiesel in a single-cylinder, 1500 rpm CI engine. Using an ANN model with injection timing and pressure, the researcher evaluates and predicts engine performance, combustion, and tailpipe emissions. At 280 bars of injection pressure and 25.5degBTDC timing, the WCPO methyl ester offers better combustion and performance parameters. To carry out the ANN training, the model was equipped with the Backpropagation learning algorithm. The input and output criteria of the MLP network were employed in the ANN model for non-linear mapping. The ANN network with two hidden layers and eleven neurones produces the exceptional correlation coefficient²³.

This ANN prediction was carried out using MATLAB software and a single hidden layer for the performance and emissions parameters of the diesel engine, based on the literature review. Two input layers, ten to nineteen neurones in the hidden levels, two neurones in the output layer, and (2-5-1-1) for performance were used to

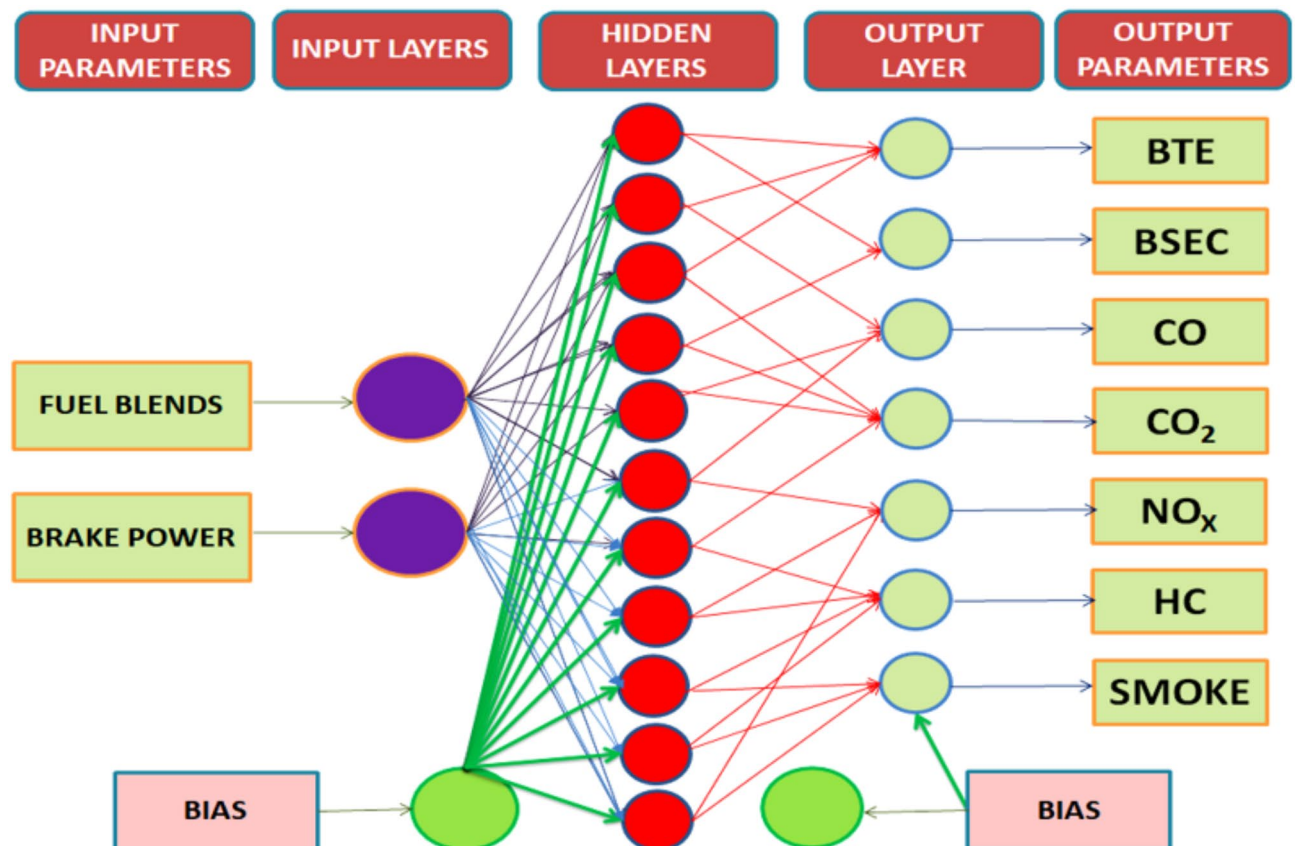


Fig. 6. Pictorial representation of artificial neural network (ANN) architecture.

develop an architecture set. In order to examine the correlation metrics, this model was put into use. To identify implementation flaws, model performance metrics and other mistakes were compared. Up till the mean square error was less than 0.01, several neurones were changed. In order to remove values that are difficult to read, one must remove the most common measurement errors, which include zeros and ambiguous values with necessary scale independence.

(e) Developed ANN model to forecast the performance and emission measurement of GGME and its mixtures.

Based on the various literature reviews, this ANN model was used for this research work. Then the statistical analysis and error measurement was estimated and performed with RSME, R^2 , MSRE, NSE, and MAPE for the evaluation of the performance of the proposed ANN model, which was displayed below:

$$\text{MAPE (Mean Absolute Percentage Error)} = \frac{1}{n} \sum_{i=1}^n \left(\left| \frac{Z_e - Z_p}{Z_e} \right| \right) \times 100 \quad (3)$$

$$R^2 \text{ (Determination coefficient)} = 1 - \left(\sum_{i=1}^n \left[\frac{(Z_e - Z_p)^2}{(Z_p)^2} \right] \right) \quad (4)$$

In these equations, n is the Experimental data, Z_e is the Experimental yield, Z_p is the predicted yield, Z_a is the Average experimental yield.

Typically, the minimum and superior value of MAPE and R^2 must be lesser than 80% to accomplish the accurate model.

$$\text{RMSE} = \sqrt{\frac{1}{n} \sum_{i=1}^n (Z_i - X_i)^2} \quad (5)$$

$$\text{MSRE} = \left[\frac{1}{n} \sum_{i=1}^n \left(\frac{Z_i - X_i}{Z_i} \right)^2 \right]_q \quad (6)$$

$$\text{NSE} = \left[1 - \left(\sum_{i=1}^n \left(\frac{Z_i - X_i}{X_i - \bar{X}} \right)^2 \right) \right]_q \quad (7)$$

The performance and tailpipe emission of raw GGME and its fuel blends with petroleum-Diesel blends were examined as BTE, BSEC and HC, CO, NO_x , CO_2 , and smoke opacity with the experimental input of fuel blends and BP. Both the Figures and Tables of the ANN model exhibits accurate, descriptive, and predicted nature of model assessed values for the experimental data of performance and emission of GGME models. The model resulted in errors also in line with the output results.

Diesel engine experimental setup and its measurements

The basic empirical study was conducted in an air-cooled, four-stroke, 5.2 kW Kirloskar brand DI Diesel engine operating at 1500 rpm. In order to conduct an experiment, the principal instrument was mounted in the engine and tested under various load conditions while maintaining a steady speed. Regular petroleum-Diesel fuel was first used to evaluate the test engine in order to excite it and obtain baseline measurements. At first, an eddy current dynamometer with a dynamometer and electrical resistance was coupled to the air-cooled test engine. It was tested with 5.2 kW of power and a steady speed of 1500 rpm. In order to monitor the pressure rise versus crank angle on a flywheel, a Kistler-made piezoelectric pressure transducer, model number 7063-A, was mounted to the test engine and coupled to a crank angle encoder. The engine was installed alongside the SES combustion analyser. The encoder, analyser, and charge amplifier made by Kistler Instrument AG in Switzerland were extremely important since they allowed the input signal from the diesel engine to be utilised by a large number of people. In order to precisely quantify the buildup of tailpipe emissions, the QROTECH Co Ltd. five gas analyser and the QRO-402 models of Korean equipment were used to measure the emissions of HC, CO, CO_2 , and NO_x . The AVL 437 C smoke opacimeter device was used to measure the emissions of smoke opacity. Figure 7 describes the Kirloskar made DI Diesel engine arrangement. During this engine test, SAE 40 lubricating oil was used to increase engine effectiveness and prevent wear and tear issues. Table 3 provided a complete specification for the diesel engine.

Uncertainty analysis of the experimental work

Numerous factors, including observations, testing standards, instrument calibration for purchased instruments, and equipment selection, would contribute to the uncertainty and inaccuracies in the instruments. In general, random mistakes and fixed errors can be used to combine uncertainty. For this uncertainty analysis, the analytical quantities are manageable. Next, the Gaussian distribution function shown in Eq. (8), along with the confidence bounds, was used to estimate the uncertainty of the evaluated parameters. The figure is known as the mean limit. About 96% of the deals in this were measured.

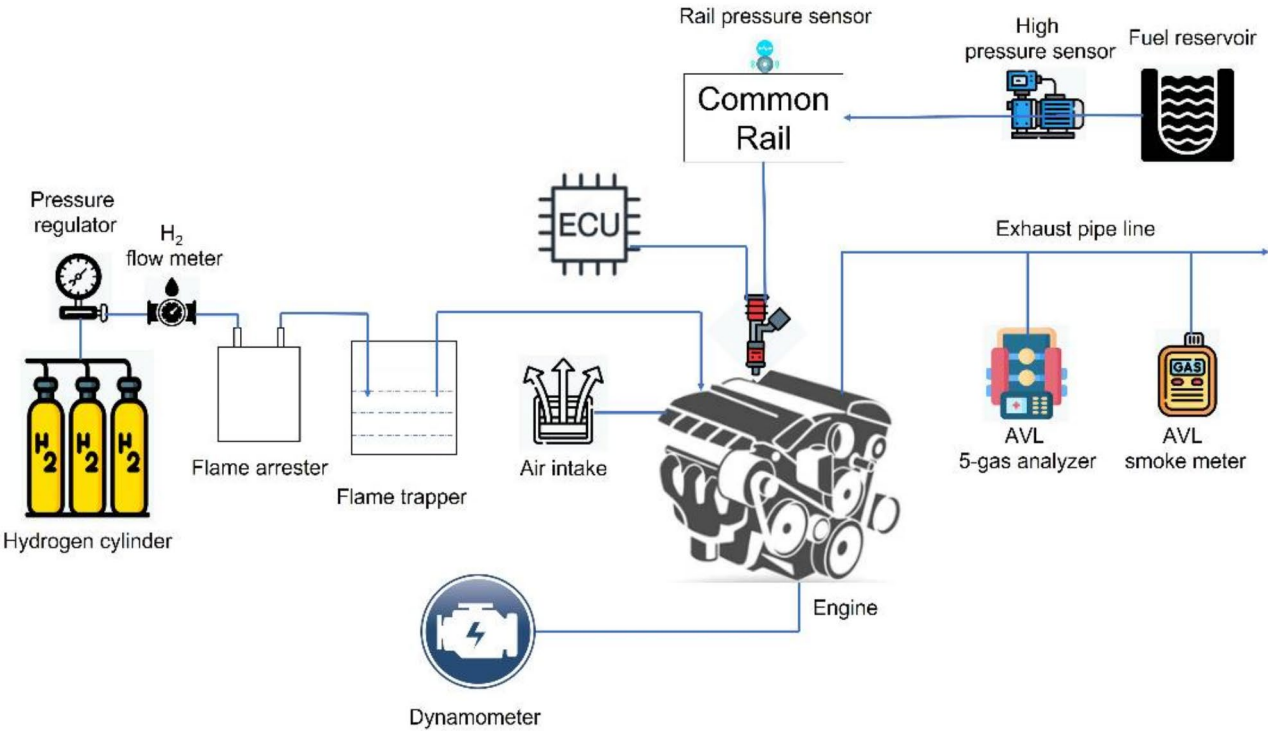


Fig. 7. Layout illustrating the diesel engine experimental setup⁵³.

Make	Kirloskar TAF-1
Type	Four stroke, single cylinder DI Diesel engine
Cooling type	Air cooled
Bore	86.6 mm
Stroke	112 mm
Compression ratio	17.6:1
Rated power and rated speed	5.2 kW at 1500 rpm
Fuel injection timing	23 deg before TDC
Fuel injection pump	MICO jerk inline type
Nozzle	0.3 mm and 1 nozzle
Piston geometry	Hemispherical
Swept volume	662 cc
The angle of fuel spray	120 deg
Lubrication system	Forced feed system
Fuel tank capacity	6.5 L
Lube oil sump capacity	3.7 L
Inlet valve open and Inlet valve close	4.5degbTDC and 35.5degaBDC
Exhaust valve open and Exhaust valve close	35.5degbBDC and 4.5degaTDC

Table 3. The detailed specification of the diesel engine.

$$\Delta Z_i = \frac{2\sigma_i}{\overline{Z_i}} \times 100 \tag{8}$$

In the above equation, the parameter $\overline{Z_i}$ is the experimental interpretations, Z_i is a number of readings, σ_i is the value of standard deviation. The estimated uncertainty of various constraints was explored as follows in Eq. (9):

$$P = f(Z_1, Z_2, Z_3, Z_4, Z_5, \dots Z_n) \tag{9}$$

Sl. No.	Used instruments	Measured range	Accuracy value	Percentage of uncertainty
1	Tachometer	0–10,000 rev/min	± 10 rpm	0.2
2	Manometer	0–200 mm	± 1 mm	1
3	Pressure transducer	0–110 bar	± 0.1 bar	0.2
4	Stopwatch	–	± 0.5 s	0.1
5	Exhaust gas temperature	0–900 °C	± 1 °C	0.12
6	Smoke meter	0–100 HSU	± 0.1 HSU	1

Table 4. Uncertainty range of several instruments used in the experiments.

Sl. No	Measured constraints	Percentage of uncertainty
1	Brake power	0.27
2	Load	0.20
3	Exhaust gas temperature	0.1
4	Brake specific energy consumption	0.1
5	Brake thermal efficiency	0.21
6	Hydrocarbon	0.3
7	Carbon monoxide	0.2
8	Carbon dioxide	0.21
9	Oxides of nitrogen	0.4
10	Smoke opacity	0.5
11	Air flow range	0.6
12	Fuel flow range	0.65

Table 5. The uncertainty of measured constraints of the diesel engine.

$$\Delta P = \sqrt{\left(\left[\frac{\partial P}{\partial Z_1} \Delta Z_1\right]^2 + \left[\frac{\partial P}{\partial Z_2} \Delta Z_2\right]^2 + \left[\frac{\partial P}{\partial Z_3} \Delta Z_3\right]^2 + \dots + \left[\frac{\partial P}{\partial Z_n} \Delta Z_n\right]^2\right)} \tag{10}$$

In the above equation, the functions $Z_1, Z_2, Z_3, \dots, Z_n$ delivers the number of readings taken from the experiment. Thence, “ ΔP ” was calculated by the root mean square and the errors related to the measured limits. Uncertainty analysis of several measuring instruments was exhibited in Table 4. The above Eq. (10) was assessed for measuring constrains and it was explored in Table 5.

Results and discussion
Nanoparticles characterization and its techniques

XRD analysis of the Fe_3O_4 nanoparticles
An equipped powered sample of Fe_3O_4 nanoparticles was exposed to XRD on a diffractometer to perceive the crystalline nature, phase status, and average grain size of Fe_3O_4 nanoparticles were exemplified in Fig. 8. The XRD patterns were noted from $2\Theta = 39.4^\circ$ active with D2 phaser XRD by Bruker operating organization by resources of CuK α (1.5406Å) radiation with a scanning rate of 5°/min. The provided voltage was established at 20 KeV and 150 mA, correspondingly. The crystallized structure of Fe_3O_4 nanoparticles was recognized by increased planes, viz. (5 1 1), (4 0 0), (4 2 2), (2 2 0), (3 1 1) and (4 0 0). In connector with these high and penetrative peaks (3 1 1) confirms the survival of Fe_3O_4 nanoparticles. The deflection peaks of Fe_3O_4 with planes (2 2 0), (3 1 1), (4 0 0), (4 2 2), (5 1 1), and (4 0 0) support the crystalline system of synthesized nanoparticles. Powerful peaks were noted in the planer of (3 1 1), and by this resource, the grain size was premeditated by using the Debye–Scherer technique, and its common grain size was ambitious to 29.22 nm. The lattice structures were discovered from the JCPDS line numbers (89–3854). By using this, it was addictive that the system is Face Centred cubic (FCC) system with mean axial ratio of 0.14 and the theoretical density of Fe_3O_4 nanoparticles, also known as magnetite were found to be 5.17 g/cm³.

Fourier transform-infrared spectroscopy (FT-IR) analysis for Fe_3O_4 and lipase immobilized Fe_3O_4
FT-IR characterization was victimized to attach the capping molecules state on the layer of nanoparticles by physiochemical technique and FT-IR absorption peaks for elegant Fe_3O_4 and lipase immobilized Fe_3O_4 , as verified in Fig. 9. An identified characteristics spot at 3412 cm^{−1} approves the existence of OH bond attached to iron oxide tangible.

This way, the NH₂ stretch was missing in the nanoparticles, and therefore, it is inferred that these compounds have to undergo reduction method while C=O bond was known at 1626 cm^{−1} the distinguishing peak at 571 cm^{−1} of Fe–O character confirms the survival of Fe_3O_4 nanoparticles in the gained sample. Lipase immobilized Fe_3O_4

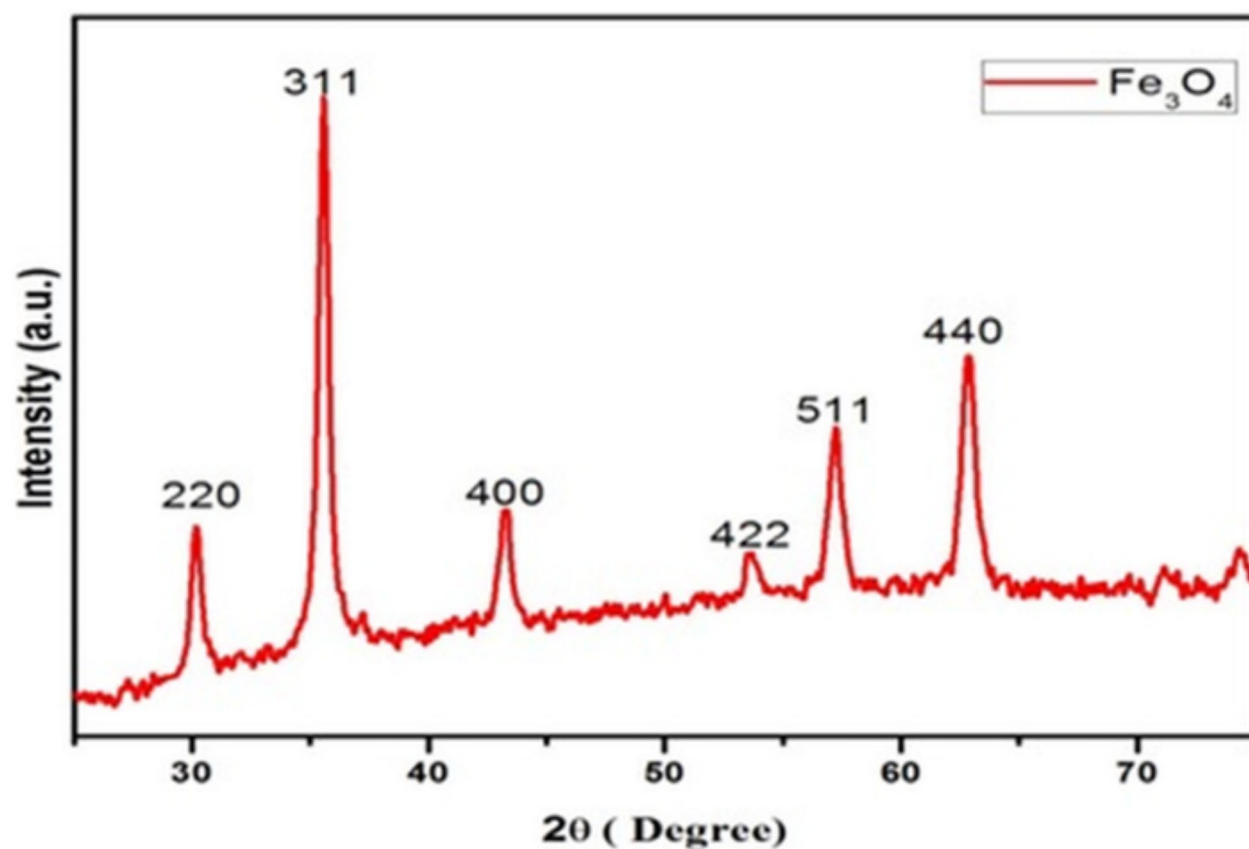


Fig. 8. X-ray diffraction pattern of Fe_3O_4 .

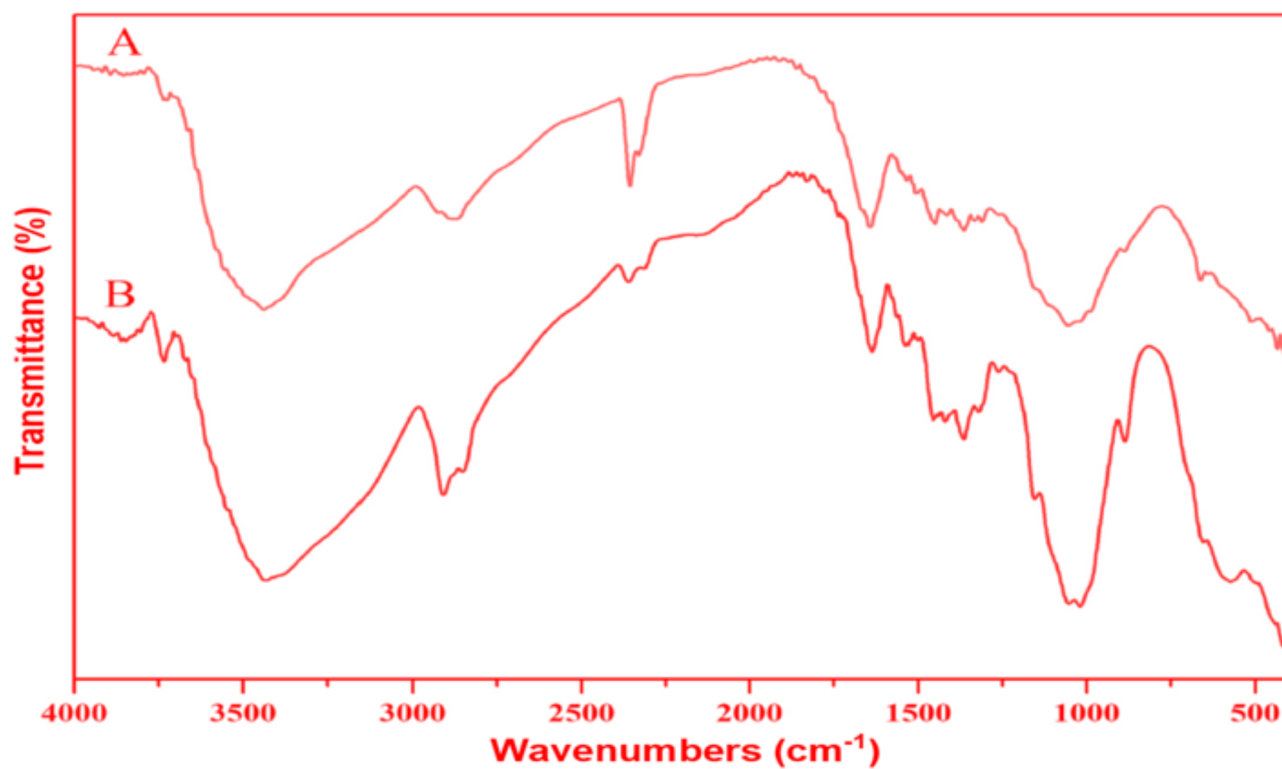


Fig. 9. (A,B) exhibit the FT-IR analysis of Fe_3O_4 nanoadditives and lipase immobilized Fe_3O_4 nanocatalyst.

peak disclosed the distribution peaks at 3326 cm^{-1} regions, and one more characteristic peak was identified at 1427 cm^{-1} . These peaks show the proximity of lipase bounded in the Fe_3O_4 nanoparticles.

Figure 10A,B shows the external morphology of Fe_3O_4 nanoparticle and immobilized Fe_3O_4 analyzed by SEM make: VEGA-3-TESCAN. Commonly, electrons reacted with atoms in the sample, and it results in different signals. These signals are treated, and an SEM image was produced. In the specific SEM images, the morphological nature of Fe_3O_4 magnetic nanoparticles exhibits roughly in nature due to the agglomeration of fine particles to magnetic coupling and the attracting nature of individual nanoparticles Fig. 10A, agglomeration and inelegance are abstracted in Fig. 10B. This result, better molecules, and binding occurred during the reaction. Figure 10A confirm the clear surface of Fe_3O_4 with 60 nanometres (nm) range, and Fig. 10B shows the more grain growth surface of immobilized Fe_3O_4 nanoparticle with 60 nm scale.

Characterization of *Garcinia* Biodiesel

FT-IR analysis of FAMEGO

To examine the FAMEGOs compound profile, the current generation high-resolution compound analyzer, FT-IR, was handled in this experimental study. The FT-IR analysis duration was 1–2 s only. The FT-IR instrument was presently preferred to examine the compound's presence in the extracted FAME GO and raw *Garcinia* seed oil from the version of the latest omnic software shown in Fig. 11A,B. The whole analysis was operated with the Nichrome source configuration, 7.3 KBr splitter, Deuteratedtriglycinesulfate-based detector installed with Magna 750 FT-IR spectrometer arrangement. The overall range of 500 to 4000 cm^{-1} with a resolution (5 cm^{-1}) was fixed in the FT-IR instrument for this analysis. The FT-IR spectrum ranges create a chemical inequity for both FAME GO, and raw *Garcinia* seed oil ranges from 3000 to 2800 cm^{-1} , named a fingerprint region.

FT-IR for extracted FAME GO produces the sharp peaks of 1721 cm^{-1} and 1843 cm^{-1} , determine the functionality of esters, acids in $\text{C}=\text{O}$ stretch, carbohydrate, and saturated fatty acid in the acquired sample. Another successive peak, 1570 cm^{-1} in the spectrum band, belongs to an amide group of compounds. Shaped peak (1321 cm^{-1}) deserves $\text{O}-\text{CH}_3$, which a glycerol-based group is attributed to FAME GO. For raw *Garcinia* seed oil samples, the FT-IR results in the existence of fatty acid groups and their compounds. Figure 11B shows sharp peaks from 2850 to 3003 cm^{-1} raised regions to agree to sp^2-CH , sp^2-CH , and aliphatic CH (hybridized alkene group). Meanwhile, 1737 cm^{-1} stretched peak related to the keto group of esters, and the 1627 cm^{-1} region is for non-keto group with unsaturated double bond availability. Numerous categorized firm peaks raised in-between 3000 and 2800 cm^{-1} area that is 3003 and 2850 cm^{-1} peaks related to the methyl ester group. Another peek at 1469 cm^{-1} in the region gives evidence of methylene groups. The other peaks, like, 1627 cm^{-1} , fit into (olefin group $\text{C}=\text{C}$), 3003 cm^{-1} for (Alkene $\text{C}-\text{H}$) that are an Aliphatic group with sp^2-CH , 1731 cm^{-1} stretch (Carbonyl single bond ester $\text{O}-\text{C}=\text{O}$) and last peak in the spectrum band 2850 cm^{-1} got Alkane ($\text{C}-\text{H}$ sp^3-CH) group.

Gas chromatography-mass spectroscopy characterization of extracted FAMEGO

GC-MS is a well-organized instrument used to scrutinize attracted FAME GO physiochemical properties from raw *Garcinia*, including finding the fatty acid profile and the compositions in a well-sophisticated manner. Also, prone to search the various carbon double chains and the fuel properties, namely, oxidation rate, combustion rate of the oils, fuel viscosity, cetane number, carbon-chain length, cold fuel property, and heating value of the biodiesel²⁴.

In general, the fatty acid configuration of the crude oil was greatly influenced by the physicochemical properties of biodiesel and evolved the knowledge of the fatty acid profile of the raw crude oil that is used to produce biodiesel. Meanwhile, biodiesel physiochemical properties are the foremost ingredient for all the fuel performance and economy. Presently, GC analysis was engaged for the extracted FAMEGO, and it discovered the available fatty acid methyl esters, fatty acids, fatty acid ratios, and other significant information. The chemical composition of *Garcinia* seed oil and comparison of fatty acid methyl ester of *Garcinia* seed oil with various fatty acid methyl esters were displayed in the Tables 6 and 7 and the GC analysis result was represented in Fig. 12.

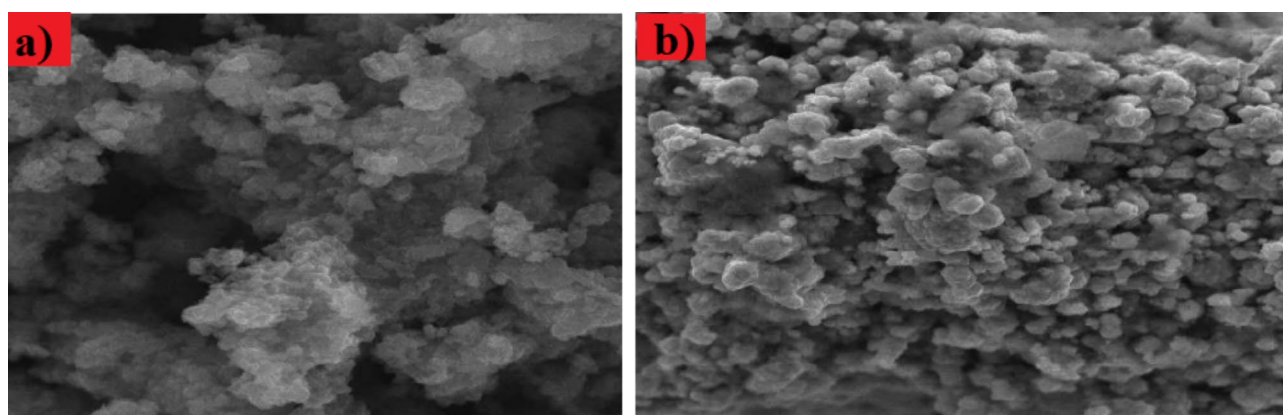


Fig. 10. (A) SEM characterization of Fe_3O_4 and immobilized Fe_3O_4 , (B) surface morphology of Fe_3O_4 nanoparticle and lipase immobilized Fe_3O_4 nanocatalyst.

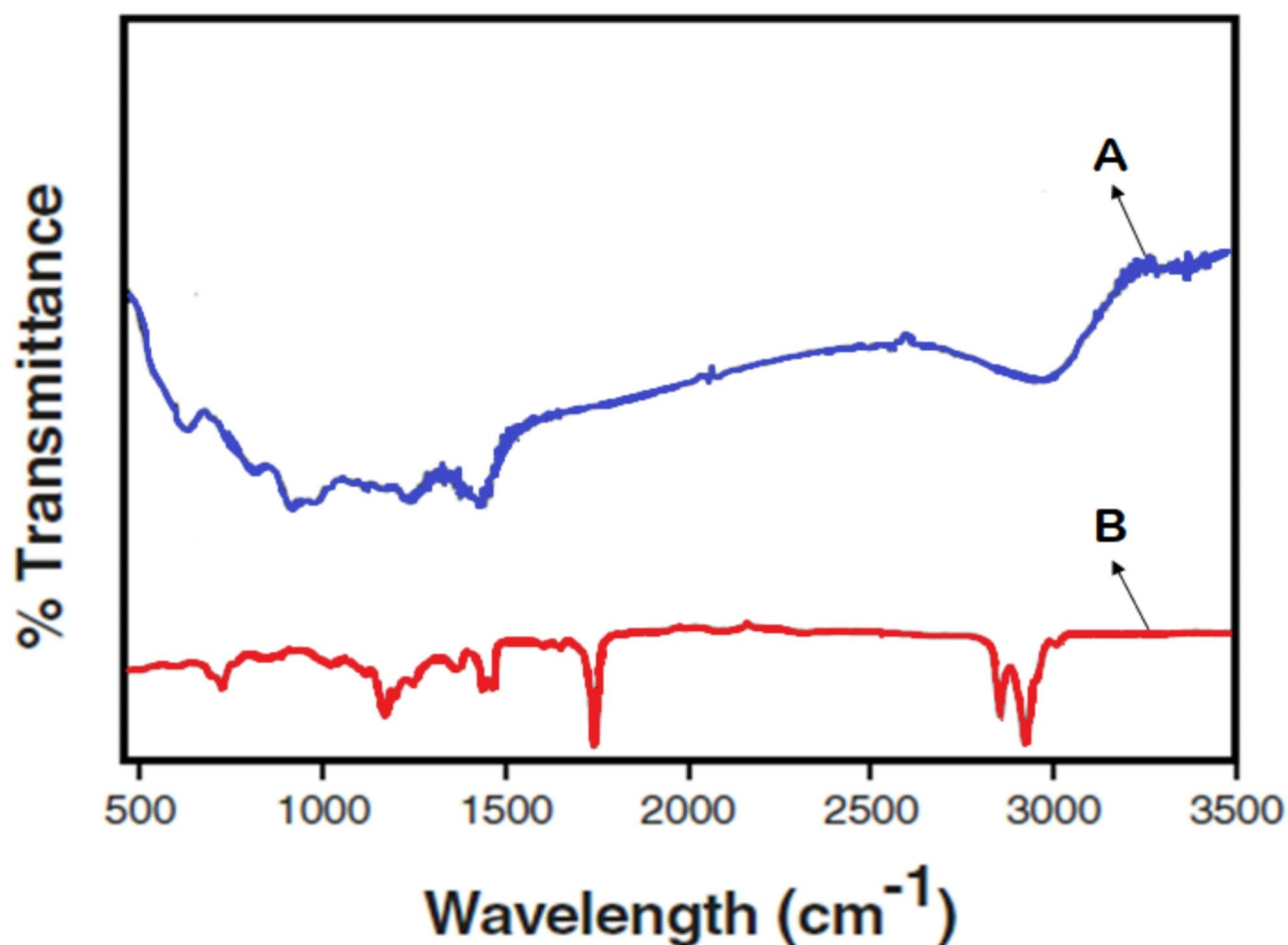


Fig. 11. (A,B) Illustrate the FT-IR spectrum of raw *Garcinia* seed oil and fames of *Garcinia*.

The fatty acid methyl ester	Fatty acid	Quantity (%)	Molecular formula	PubChem CID/CAS	IUPAC name	Class of compound
10,13-trimethyl myristate	Myristic acid (C14:0)	0.05	C ₁₇ H ₃₄ O ₂	267650-23-7	Tetradecanoic acid,10,13-dimethyl-, methyl ester	Saturated
Methyl linoleate	Linoleic acid (C18:2n6c)	3.92	C ₁₉ H ₃₄ O ₂	900336-44-2	Methyl 10-trans, 12-cis-octadecadienoate	Poly-unsaturated
Methyl oleate	Oleic acid (C18:1n9c)	52.68	C ₁₉ H ₃₆ O ₂	900336-41-6	Methyl13-octadecenoate	Mono-unsaturated
16-dimethyl margarate	Margaric acid (C17:0)	2.11	C ₁₉ H ₃₈ O ₂	900336-38-6	Methyl 16-methyl-heptadecanoate	Saturated
Methyl arachidate	Arachidic acid (C20:0)	1.29	C ₂₁ H ₄₂ O ₂	1120-28-1	Methyl eicosanoate	Saturated
Methyl stearate	Stearic (C18:0)	7.02	C ₁₈ H ₃₆ O ₂	5281-57-11-4	Octadecanoate	Saturated
Methyl palmitate	Palmitic (C16:0)	10.75	C ₁₇ H ₃₄ O ₂	985-57-10-3	Hexadecanoic acid	Saturated
Methyl elaidate	Elaidic (C18:1n9t)	0.057	C ₁₈ H ₃₄ O ₂	637517-2027-7-6	(E)-octadec-9-enoic acid	Unsaturated
Methyl behenate	Behenic (C22:0)	3.73	C ₂₂ H ₄₄ O ₂	8215-112-85-6	Docosanoic acid	Saturated
Methyl linelaidate	Linolelaidic (C18:2n6t)	0.89	C ₁₈ H ₃₂ O ₂	5282457-506-21-8	9E,12E-octadeca-9,12-dienoic acid	Unsaturated
Eicosenoic acid methyl ester	Eicosenoic (C20:1n9)	1.124	C ₂₀ H ₃₈ O ₂	5282769-2462-94-4	E-icos-11-enoic acid	Mono unsaturated
Methyl myristoleate	Myristoleic	–	C ₁₄ H ₂₆ O ₂	5281119-544-64-9	Z-tetradec-9-enoic acid	Mono unsaturated
Methyl linoleate	Linolenic (C18:3n6)	3.87	C ₁₈ H ₃₀ O ₂	5280934-463-40-1	9Z,12Z,15Z-octadeca-9,12,15-trienoic acid	Poly unsaturated
Methyl margarate	Margaroleic (C17:1)	0.065	C ₁₇ H ₃₂ O ₂	5282748-1981-50-6	Z-heptadec-9-enoic acid	Unsaturated
Methyl laurate	Lauric (C12:0)	0.037	C ₁₂ H ₂₄ O ₂	3893-143-07-7	Dodecanoic acid	Saturated
Methyl palmitoleate	Palmitoleic (C16:1)	–	C ₁₆ H ₃₀ O ₂	445638-373-49-9	Z-hexadec-9-enoic acid	Unsaturated

Table 6. Chemical composition of raw *Garcinia* seed oil⁵².

Fatty acids	Raw <i>Garcinia</i> seed oil	<i>Jatropha</i>	<i>Jatropha gossypifolia</i>	<i>Calophylluminophyllum</i>	<i>Meynaspinos</i> Roxb.Ex.
Myristic acid (C14:0)	0.05	0.42	4.3	0.09	–
Linoleic acid (C18:2n6c)	3.92	0.87	19.3	26.33	52.533
Oleic acid (C18:1n9c)	52.68	45.2	22.45	37.57	30.251
Margaric acid (C17:0)	2.11	–	–	–	0.206
Arachidic acid (C20:0)	1.29	0.6	–	0.8	1.449
Stearic (C18:0)	7.02	6.23	10.37	8.42	5.23
Palmitic (C16:0)	10.75	15.12	26.78	12.05	7.08
Elaidic (C18:1n9t)	0.057	–	–	–	–
Behenic (C22:0)	3.73	–	–	–	0.289
Linolelaidic (C18:2n6t)	0.89	–	–	–	0.213
Eicosenoic (C20:1n9)	1.124	–	–	–	1.152
Myristoleic	–	–	–	0.89	1.338
Linolenic (C18:3n6)	3.87	0.079	–	0.28	0.378
Margaroleic (C17:1)	0.065	–	–	3.01	–
Lauric (C12:0)	0.037	0.2	9.75	–	–
Palmitoleic (C16:1)	–	0.899	–	0.34	–
Overall saturated	39.68	21.23	51.2	16.25	15.46
Overall polyunsaturated	15.23	31.22	19.17	37.36	38.45
Overall monounsaturated	45.09	78.6	21.8	33.08	82.541

Table 7. Fatty acid methyl ester of raw *Garcinia* seed oil and other type of oils⁵².

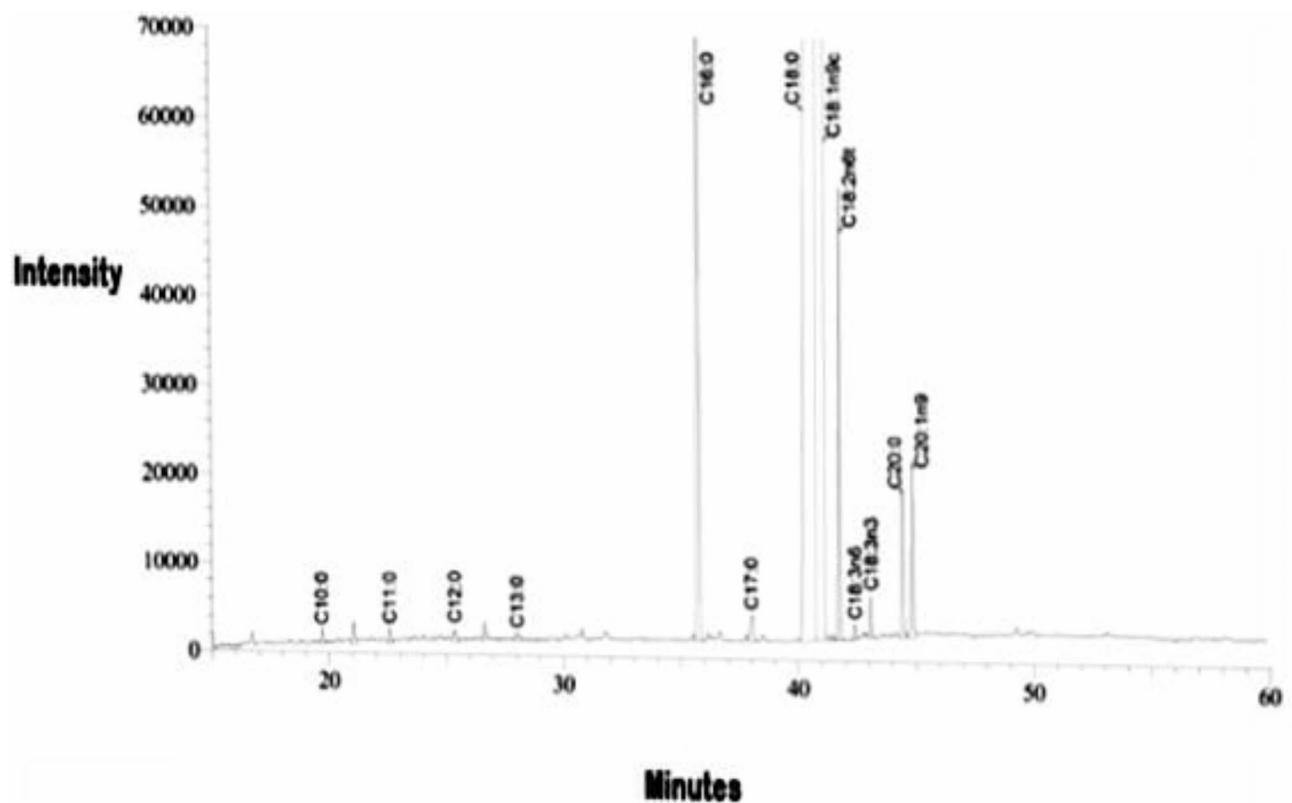


Fig. 12. GC analysis of extracted *Garcinia* FAME peaks.

Figure 12 shows that the GC analyzer generates various peaks related to relative abundance (%) versus Time (min) deals with extracted FAMEGO. As pertaining to further peaks, 39.09% and 35.69% stretch was sharper and broad peaks in the graph. The peak 35.69% shows (E)—methyl octadec—13 enoate related to oleic acid and additional peak 39.69% stretch equivalent for methyl 16—methyl heptadecanoate it known as margaric acid and

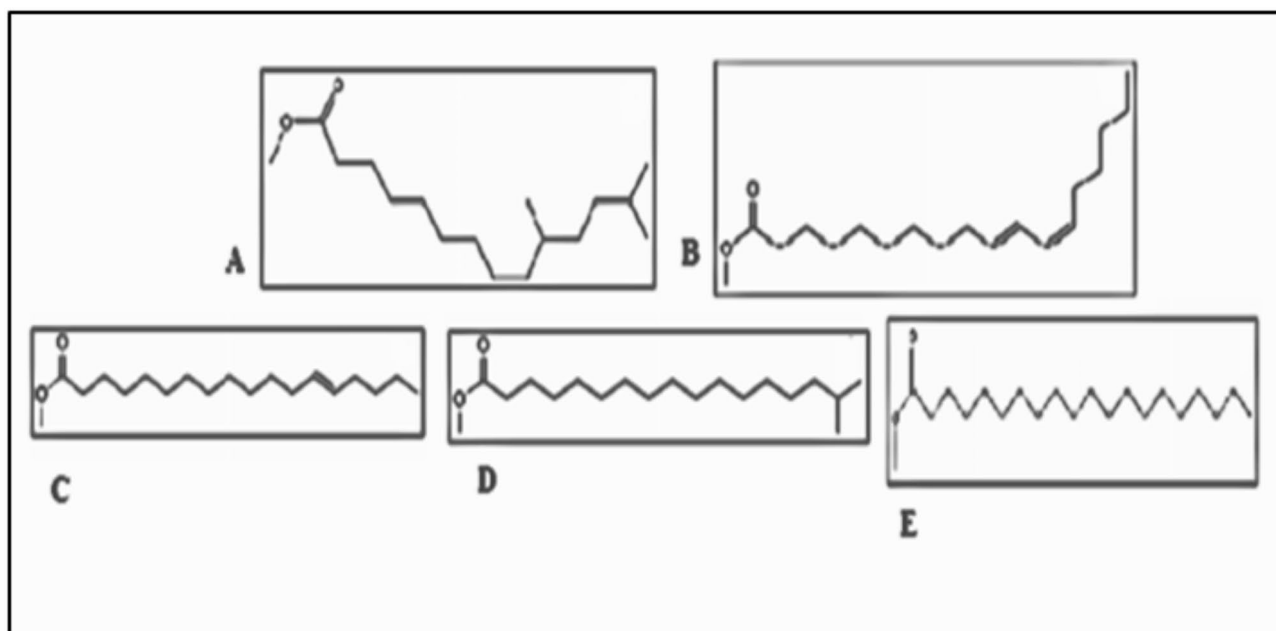


Fig. 13. Mass spectroscopy structure of extracted *Garcinia* FAME molecules⁵².

Colour	White
Average particle size (nm)	19–24
Purity (%)	96.99
Specific surface area (m ² /g)	372
Bulk/ true density (g/cc)	0.18
Microstrain (ξ)	0.084
Dislocation density (δ) (line ² /m ²)	0.5×10^{14}

Table 8. Properties of synthesized TiO₂ nanoparticles⁵¹.

other peaks results, myristic acid, linoleic and arachidic acid consistently. Commonly, unsaturated fatty acids presented in the raw oils results in a lower level of biodiesel production.

Mass Spectroscopy (MS) is an instrument specialized to determine the structures and compounds exposed in the extracted oil samples. It works in the mechanism of NIST, which generates ion peaks correlated to the molecules. THE extracted FAME GO sample was located in the MS, then the β -carbon atoms were developed by the instrument, and the β -carbon atoms were permitted to pass over the FAME GO molecules.

Hence, it possesses an MC Lafferty molecular rearrangement spectrum. This spectrum had a gathering of all mass fragmentation linked to the sample compounds. These collections of fragment patterns were recorded by mass spectroscopy, and based on the design, the structure and compounds were estimated from the FAME GO molecules, and it is exemplified in Fig. 13. As defined in Fig. 13, the structure A—10, 13-trimethyl myristate, B—Methyl linoleate, C—Methyl oleate, D—16-dimethyl margarate, and E—Methyl arachidonate compound. These are the IUPAC names of the essential components that are presented in the extracted FAME GO.

Synthesis and characterization of TiO₂ nanoparticles

The process commences with the treatment of titanium tetraisopropoxide, the precursor material, using ethanol, hydrochloric acid, and deionized water. The resulting mixture underwent stirring for 30 min until it attained a pH of 1.5. Following that, 10 mL of deionized water was introduced, and the stirring continued at room temperature for 2 h, eventually reaching a pH of 6. Further titration with deionized water led to the formation of cladigel, with a pH of 8. Subsequently, the cladigel was dried and subjected to calcination at 150 °C for 12 h. Lastly, the TiO₂ nanoparticles were obtained by subjecting the dried samples to a temperature of 300 °C for 2 h. The physical properties of the synthesized TiO₂ nanoparticles are elaborated in Table 8. HR-TEM and TEM morphology (Fig. 14a,b) carried out using the JEM-3010 ultra-high-resolution analytical electron microscope revealed distinct lattice fringes, indicating the presence of nanocrystalline TiO₂ particles. The SEM image (Fig. 14c) obtained using the VEGA3-TESCAN preparation showed an irregular spherical distribution of nanoparticles with slight aggregation.

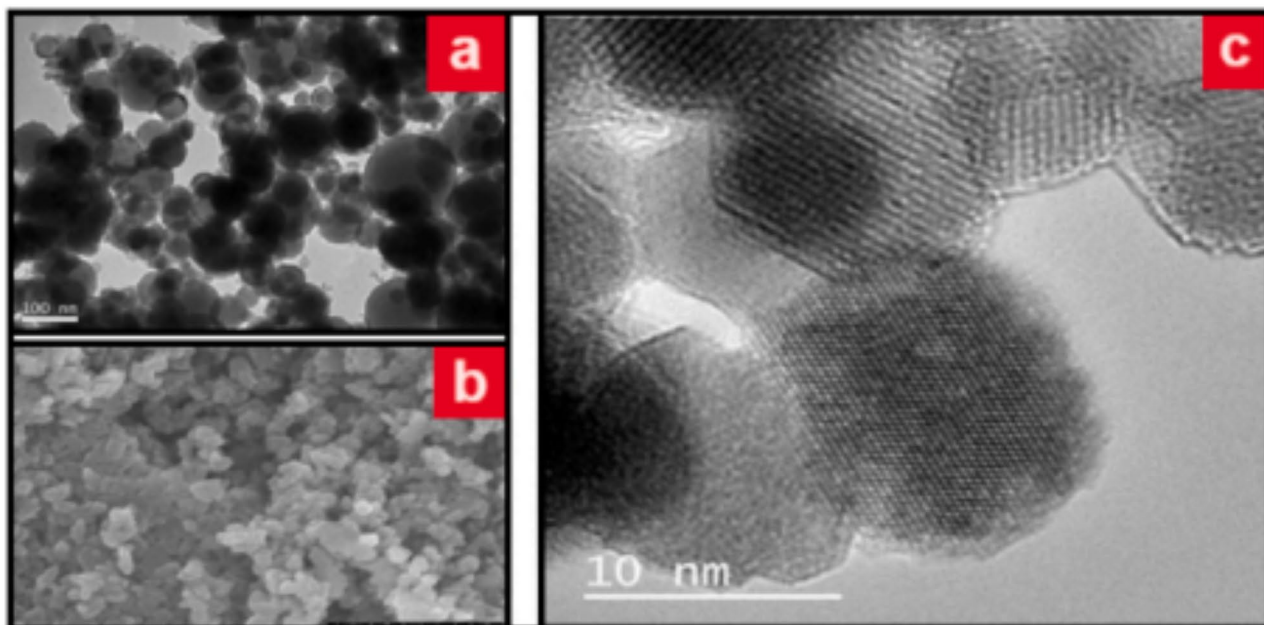


Fig. 14. (a) HR-TEM, (b) TEM, (c) SEM of TiO_2 ⁵¹.

Engine characteristics

This four-stroke, single-cylinder, water-cooled compression ignition engine was used for all of the testing. To ensure unambiguous findings, the CI engine was driven for 10 min without fuel after the nanocatalyst mixed biofuel was obtained. This was done in preparation for conducting experimental tests. The various gasoline mixes, including Diesel, B10, B20, Diesel- TiO_2 , B10- H_2 - TiO_2 , and B20- H_2 - TiO_2 , were tested for each one. The dynamometer has the engine attached to it. The data procured through PC was linked to an AVL gas analyzer, which was utilized in that configuration to obtain the emission patterns²¹. To obtain performance data, a PC with the performance measuring system installed was used. To regulate H_2 gas supply, a filter was utilized. Through the conveyance of the data to PC, the data logger was used to calculate the data. Table 1 enumerates the Physico-chemical properties of the test fuels. According to Tables 2 and 3 every test was carried out at a different engine speed ranging from 1800 rpm to 2200 rpm.

Performance characteristics

Torque

Each test fuel (Diesel, B10, B20, Diesel- TiO_2 , B10- H_2 - TiO_2 , and B20- H_2 - TiO_2) provided the same amount of engine torque. As the engine speed increases, the torque produced decreases, as seen in Fig. 15. This occurs as a result of both incomplete combustion and disrupted air intake at faster speeds. The torque at high speeds is therefore decreased by the increasing pressure. Yet, the B10- H_2 - TiO_2 fuel blend produced more torque (21.3 N-m) than other fuel blends when a 5 lit/min hydrogen supply was applied at a slower speed of 1800 rpm. Diesel- TiO_2 , B10- H_2 - TiO_2 , B20- H_2 - TiO_2 , DIESEL, B10 and B20 blend possesses torque of about 21.8, 21.3, 20.5, 19.5, 20.1, and 19.5 Nm at low engine speed. Engine torque was improved by 6% and 5% for B10- H_2 - TiO_2 and B20- H_2 - TiO_2 , respectively, when hydrogen and TiO_2 were added to the normal blend. Figure 16 also shows that the engine's torque was increased by the addition of hydrogen and nanoparticles. Torque decreased dramatically as engine speed rises.

For example, between lower engine speeds and 2800 rpm, the torque loss for the blends Diesel, B10, B20, Diesel- TiO_2 , B10- H_2 - TiO_2 , and B20- H_2 - TiO_2 was 24%, 27%, 28%, 28%, 26%, and 27%. Due to the significant decrease in thermal efficiency, torque has drastically decreased.

Brake thermal efficiency (BTE)

The BTE values for all gasoline blends—Diesel, B10, B20, Diesel- TiO_2 , B10- H_2 - TiO_2 , and B20- H_2 - TiO_2 at various engine speeds from 1800 rpm till 2700 rpm were displayed in Fig. 16. The diagram illustrates the basic fact that an increase in engine speed lowers the BTE in a manner akin to the torque pattern of the test engine. The Diesel fuel produced a higher BTE at 1800 rpm than the B10 and B20 fuel without the influence of hydrogen or nanoparticles. B10 and B20 blends had BTEs of 21.5% and 21%, respectively, but pure DIESEL had a BTE of 24%. By adding nanoparticles to fuel mixes with hydrogen supply as Diesel- TiO_2 , B10- H_2 - TiO_2 , and B20- H_2 - TiO_2 , the corresponding percentages at 1800 rpm were 24.2%, 22%, and 21.6%, respectively. The highest BTE value was obtained by the biofuel blend B10 due to combined influence of nanoparticles with hydrogen resulted in a reduced viscosity. The increased BTE is caused by the hydrogen's stronger diffusivity and faster flame⁴¹. With nanoparticle addition in biofuel, the BTE is found to increase in several literatures (Attia et al.⁵⁴; Arockiasamy & Anand⁵⁵; Aalam & Saravanan⁵⁶; Shaafi & Velraj⁵⁷; Anbarasu et al.⁵⁸). However, some contradictory results with

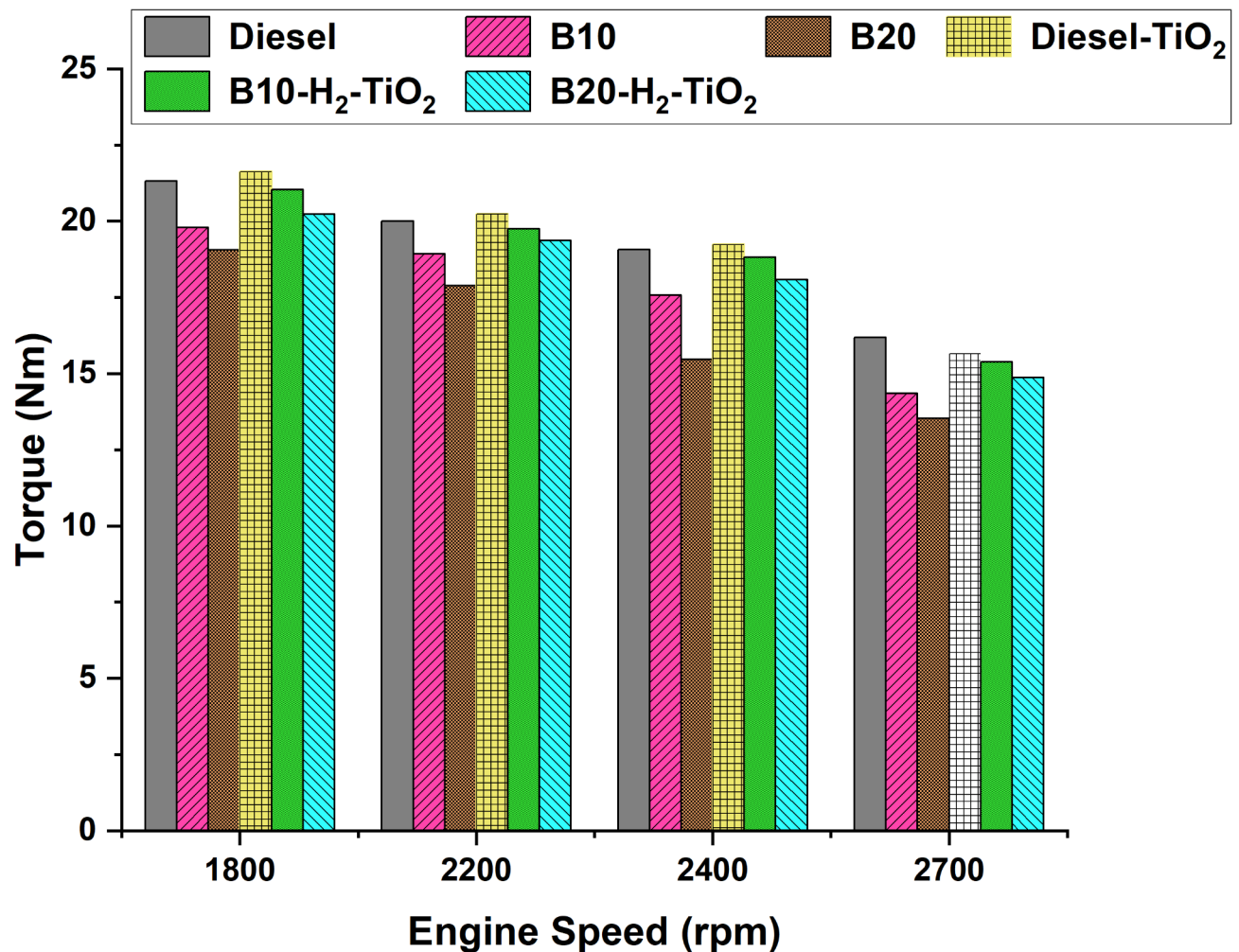


Fig. 15. Variation of torque with respect to engine speed.

higher nanoparticles giving rise to lowered BTE were reported in few literatures (Prabu & Anand⁵⁹; Sharma et al.⁶⁰). Additionally, hydrogen has a reduced quenching distance. In addition, the BTE is increased by the nanoparticles, which are vital. One more factor contributing to a full combustion and the BTE rise is the increasing oxygen content and decreased viscosity. The fuel Diesel, B10, B20, Diesel-TiO₂, B10-H₂-TiO₂, and B20-H₂-TiO₂ exhibited a progressive decrease in BTE values at 2400 rpm and 2700 rpm. However, the maximal hydrogen supply with nanoparticles at each speed produced the highest values (Fig. 17).

Brake specific fuel consumption (BSFC)

Regarding the BSFC, the result is the reverse of the BTE. A higher BSFC results from faster speeds. In addition, at lower engine speeds (especially 1800 rpm), the BSFC range of Diesel, B10, and B20 were about 421, 382 and 358 g/kW-h. The minimum value for B20's specific fuel usage was this. In addition, the BSFC decreased at all speeds as the percentage of hydrogen and TiO₂ particles increased. The significantly reduced value of BSFC, 349 g/kWh, was obtained, particularly for the fuel blend B20-H₂-TiO₂. Similar reductions in BSFC with nano additives were also quoted by several researchers (Prabu and Anand⁵⁹; Shaafi and Velraj⁵⁷; Patel and Kumar⁶¹).

With increasing nanoparticle concentration, the BSFC is found to decrease.

in the literatures of Attia et al.⁵⁴; Arockiasamy and Anand⁵⁵; Aalam and Saravanan⁵⁶; Shaafi and Velraj⁵⁷ and Anbarasu et al.⁵⁸. However, some contradictory results with higher nanoparticles giving rise to higher BSFC were reported such as Prabu and Anand⁵⁹; Sharma et al.⁶⁰ which could be attributed to prolonged ignition delay along with shorter spray penetration causing poor combustion efficiency. While the engine speed rose, the BSFC values showed a considerable increase in fuel consumption^{42,43}. At lower speeds, the BSFC data was lesser for Diesel-TiO₂, B10-H₂-TiO₂, and B20-H₂-TiO₂ (421, 382, 358, 403, 368, and 344 g/kW-h). The full combustion and increased heating value brought about by the blending of nanoparticles and hydrogen are responsible for the BSFC decrease. It is comparatively, cost-effective in comparison with Diesel with surplus H₂ supply or even pure Diesel (excluding additives) since B20-H₂-TiO₂ has a lower brake-specific fuel consumption⁴⁴.

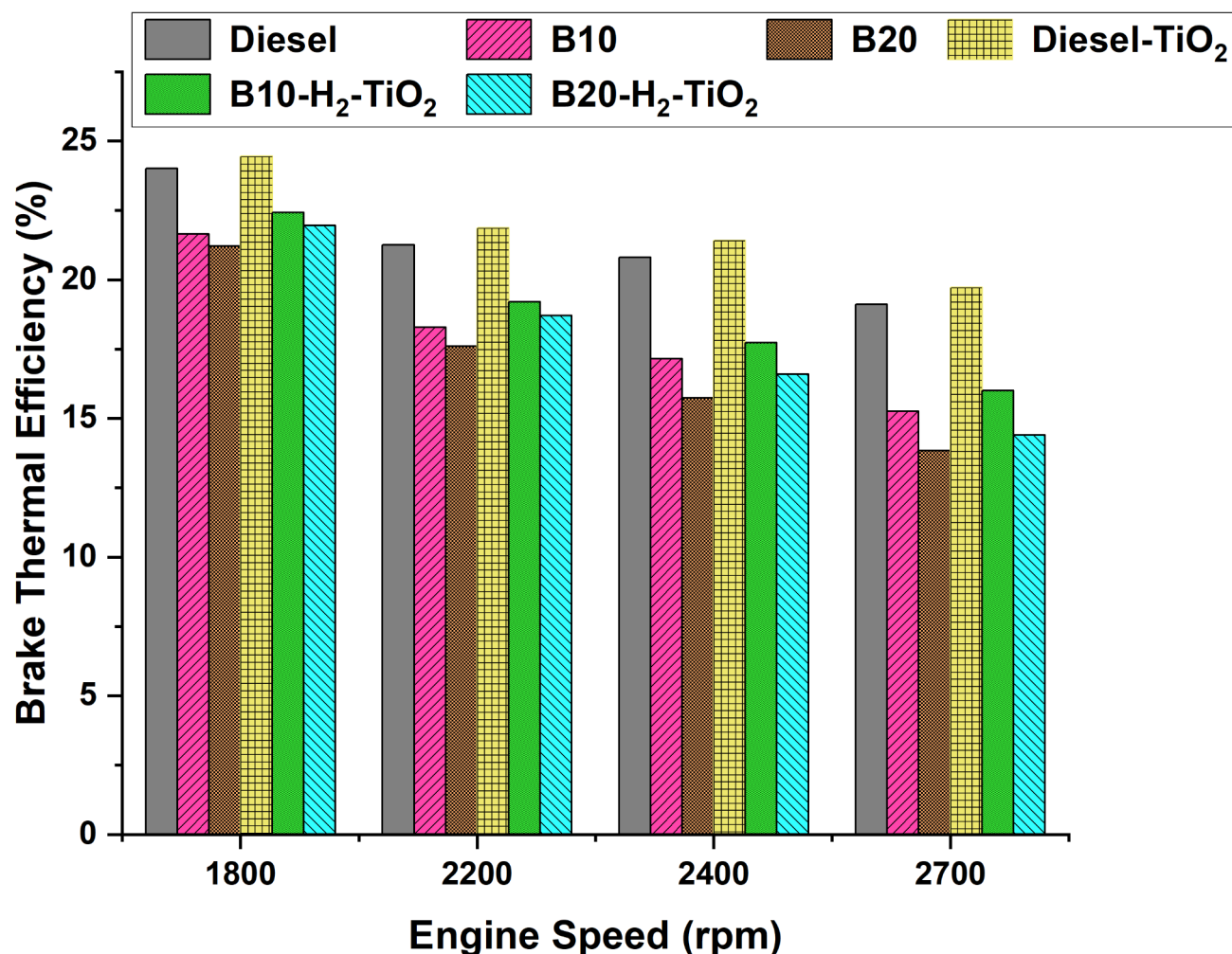


Fig. 16. Variation of brake thermal efficiency (BTE) with respect to engine speed.

Emission characteristics

Upon experimentation for the blends of Diesel, B10, B20, Diesel-TiO₂, B10-H₂-TiO₂, and B20-H₂-TiO₂ the following figures illustrate the varying emission rates of carbon monoxide, Carbon dioxide, and nitrous oxides at various engine operating speeds from 1800 rpm till 2700 rpm. Emission rates from fuel must be measured in order to prevent the greenhouse effect from getting worse.

Carbon monoxide (CO) emission

Figure 18 displays the value of CO emission for several gasoline mixes (Diesel, B10, B20, Diesel-TiO₂, B10-H₂-TiO₂, and B20-H₂-TiO₂) at various engine speeds. It is clear from the figure that the addition of hydrogen and nanoparticles reduces the amount of CO. This is due to the fact that an increase in biofuel will result in an increase in oxygen content⁴⁵. Similar studies with Al₂O₃ nanoparticles addition lowering the CO emissions were shown by several researchers (Shaaifi and Velraj⁵⁷; Sivakumaret al.⁶²; Hosseini et al.⁶³). With increasing nanoparticle concentration, the CO is found to decrease in the literatures of Attia et al.⁵⁴, Gumus et al.⁶⁴, Arockiasamy and Anand⁵⁵ and Chandrasekaran et al.⁶⁵. However, some contradictory results with higher nanoparticles giving rise to higher CO were reported such as Kannan et al.⁶⁶, and Aalam and Saravanan⁵⁶ which is possibly due to the hindering of oxidation process with more nanoparticles stopping CO oxidation to CO₂ molecule and stays as CO itself. The biofuel's higher oxygen content, the addition of nanoparticles that reduce viscosity, and the addition of hydrogen that increases diffusivity and flame speed all contribute to a clearer combustion rate that leaves no fuel unburned. The CO emissions are also caused by the fuel's unburned components. Furthermore, because hydrogen lacks the carbon structure, it emits less CO. Full combustion is also made possible by the TiO₂'s large energy surface area. Conversely, when the speed is increased, so did CO emissions. Fuel mixes Diesel-TiO₂, B10-H₂-TiO₂, and B20-H₂-TiO₂ had CO levels of 0.079, 0.043, 0.06, 0.081, 0.044, and 0.387% vol. at 1800 rpm, respectively. Compared to standard blends of B10 and B20, the emission of CO values was greater with the hydrogen supply.

The blends containing hydrogen B10-H₂-TiO₂ exhibited a 2% increase in hydrogen generation as compared to B10. However, the B20-H₂-TiO₂ reported 25% lower CO emissions than the B20, which is only attributable to

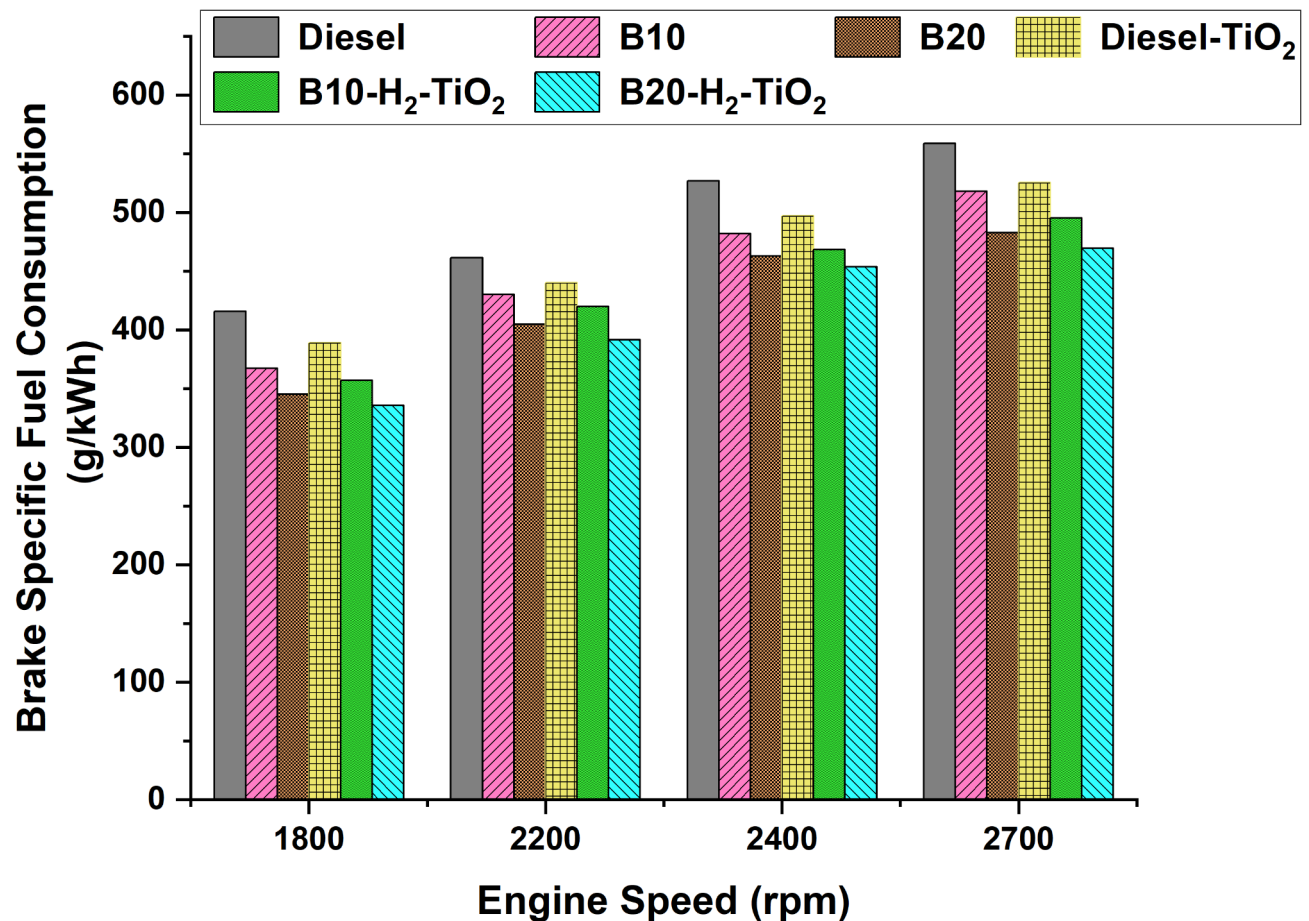


Fig. 17. Variation of brake specific fuel consumption (BSFC) with respect to engine speed.

the fuel burning through to the end. Higher concentrations of biodiesel resulted in a significant decrease in CO emissions. Hydrogen added to the biofuel blends and pure Diesel reduced CO by an average of 26%.

Carbon dioxide (CO₂) emission

The CO₂ emission as a function of engine speed is shown in Fig. 19. While CO₂ emissions rise with speed, at a certain point in time, clean Diesel and biofuel blends containing hydrogen and nanoparticles as well as fuels without additives—such as DIESEL, B10, and B20 have showed higher CO₂ emissions⁴⁶. For instance, at lesser engine speeds, the CO₂ emissions of Diesel, B10, and B20 was found to be 4.2%, 3.8%, and 3.5%, respectively, whereas the CO₂ emissions of Diesel-TiO₂, B10-H₂-TiO₂, and B20-H₂-TiO₂ were only 4.2%, 3.7%, and 3.5%, respectively, significantly lower than the plain fuel mixes. According to the research, running an engine at a fast speed causes a higher percentage of full combustion, which increases the release of CO₂ and other gases that are comparable to CO³². Because of the carbon concentration of the biodiesel mixes, there has been an increase in emissions. Since hydrogen gas doesn't contain carbon molecules, adding hydrogen to biodiesel decreased the amount of CO that was released.

Nitrogen oxides (NO_x) emission

Figure 20 displays the variation of nitrogen oxides emissions of Diesel, B10, B20, Diesel-TiO₂, B10-H₂-TiO₂, and B20-H₂-TiO₂ at various. NO_x emissions, in fact, rises in tandem with increased velocity. It results from the higher temperature of combustion. The emission of NO_x is enhanced not only by increasing speed but also by including hydrogen⁴⁷. The reason for the elevated cylinder temperature can be attributed to the elevated calorific value of hydrogen. With increasing nanoparticle concentration, the NO_x emissions are found to decrease in the literatures of Attia et al.⁵⁴, Gumus et al.⁶⁴, Arockiasamy and Anand⁵⁵, and Chandrasekaran et al.⁶⁵. However, some contradictory results with higher nanoparticles giving rise to higher NO_x emissions were reported such as Shaafi and Velraj⁵⁷, Mohan et al.⁶⁷ and Prabu and Anand⁵⁹. This is due to the fact that, the oxygen buffering tendency of nanoparticles getting shattered with higher viscous blend which along with higher in-cylinder temperatures promoting the O₂ and N₂ mixing followed by higher NO_x emission. The NO_x emission increases in conjunction with the cylinder temperature peak^{48,49}. Diesel, B10, and B20 plain fuels had NO_x emissions of 220 ppm, 350 ppm, and 560 ppm, respectively; in contrast, fuel blends with hydrogen and nanoparticles added, B10-H₂-TiO₂ and B20-H₂-TiO₂, reported NO_x reductions of 20 ppm and 30 ppm compared to B10 and B20. Figure 20 shows that the temperature rise for NO_x emission is the major factor to take into account in this situation.

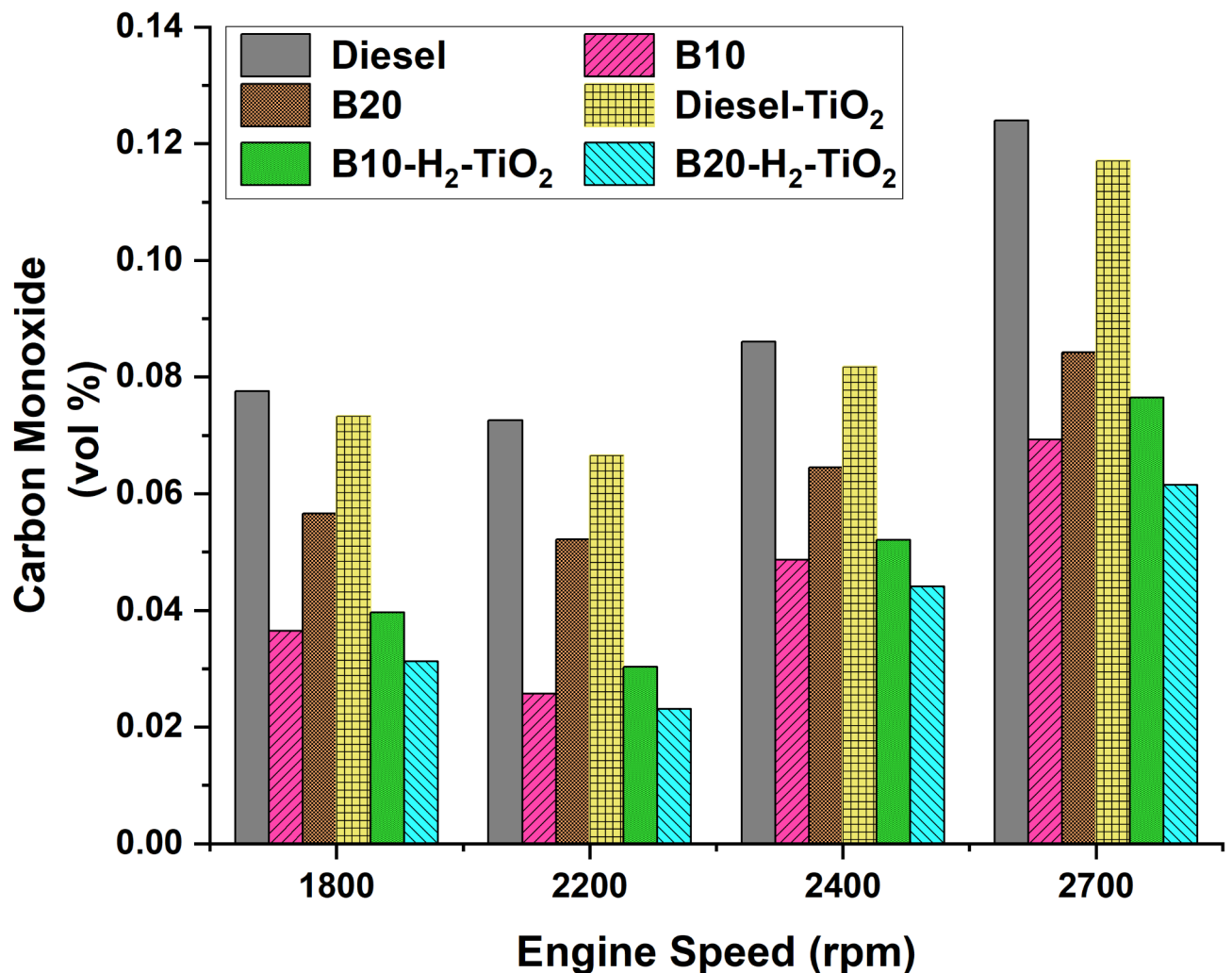


Fig. 18. Variation of carbon monoxide (CO) emission with respect to engine speed.

Proposed ANN model validation and its analysis of the GGME fuelled engine output

The Diesel engine experimental work was performed based on the design matrix output, which was designed and developed by experiment software design its details were displayed in Table 9. Then the ANN model was used to optimize and predict the experimental data's (Diesel engine output) and for this ANN model, Diesel engine brake power, biodiesel, and its fuel blends, Diesel fuel was assigned as an input parameter, and the BTE, BSFC, CO, CO₂ and NO_x emissions were assigned as an output parameter³⁷.

Then the Diesel engine experimental work results, *Garcinia* B20 fuel blend generate 8.08% drop in BTE compared to petroleum-Diesel, and mineral Diesel holds lesser energy consumption rate but B20 blend yield higher energy consumption range by its properties like calorific value and viscosity. In the case of emissions correlated with other fuel blends, B10 and B20 blends punch lowered rate of 8.39% and 10.35% with petroleum-Diesel at topmost load condition. Both B20 and Diesel-TiO₂ blends hold significantly reduced CO emissions of 18.42% and 19.20% with petroleum-Diesel, and this could be owing to the higher carbon chain length of GGME fuel, lessened viscosity, and density. Compared with mineral Diesel fuel, the B10 and B20 fuel blends result in a higher range of CO₂ emissions at peak load conditions, and B10 and B20 blends have 700 ppm and 744 ppm of higher NO_x emissions related to mineral Diesel fuel at higher load condition.

The ANN model error and performance was tabulated in Table 10. The Fig. 21a,b reveals the experimental, prediction and optimization of the Diesel engine performance (BTE and BSEC) and its R², RMSE and R value for BSEC (0.99373, 0.250301 and 0.9996) and BTE (0.992448, 0.419935 and 0.993). From these results, the R value had better accuracy rate for the Diesel engine performance model with an RMSE lesser value. Next, Fig. 22c–e display the predicted, optimized and experimental result of CO, CO₂ and NO_x emissions with the R², RMSE and R values are HC (0.995783, 0.635321 and 0.99587), CO (0.964267785, 0.002488626 and 0.9983), CO₂ (0.997672579, 0.031630703 and 0.99725), NO_x (0.984559489, 44.89075405 and 0.9847) and smoke emission (0.986814591, 1.00294331 and 0.9990). Moreover, the RSME had lowered rate of percentage error which was related with R value of the ANN model result^{38,39}.

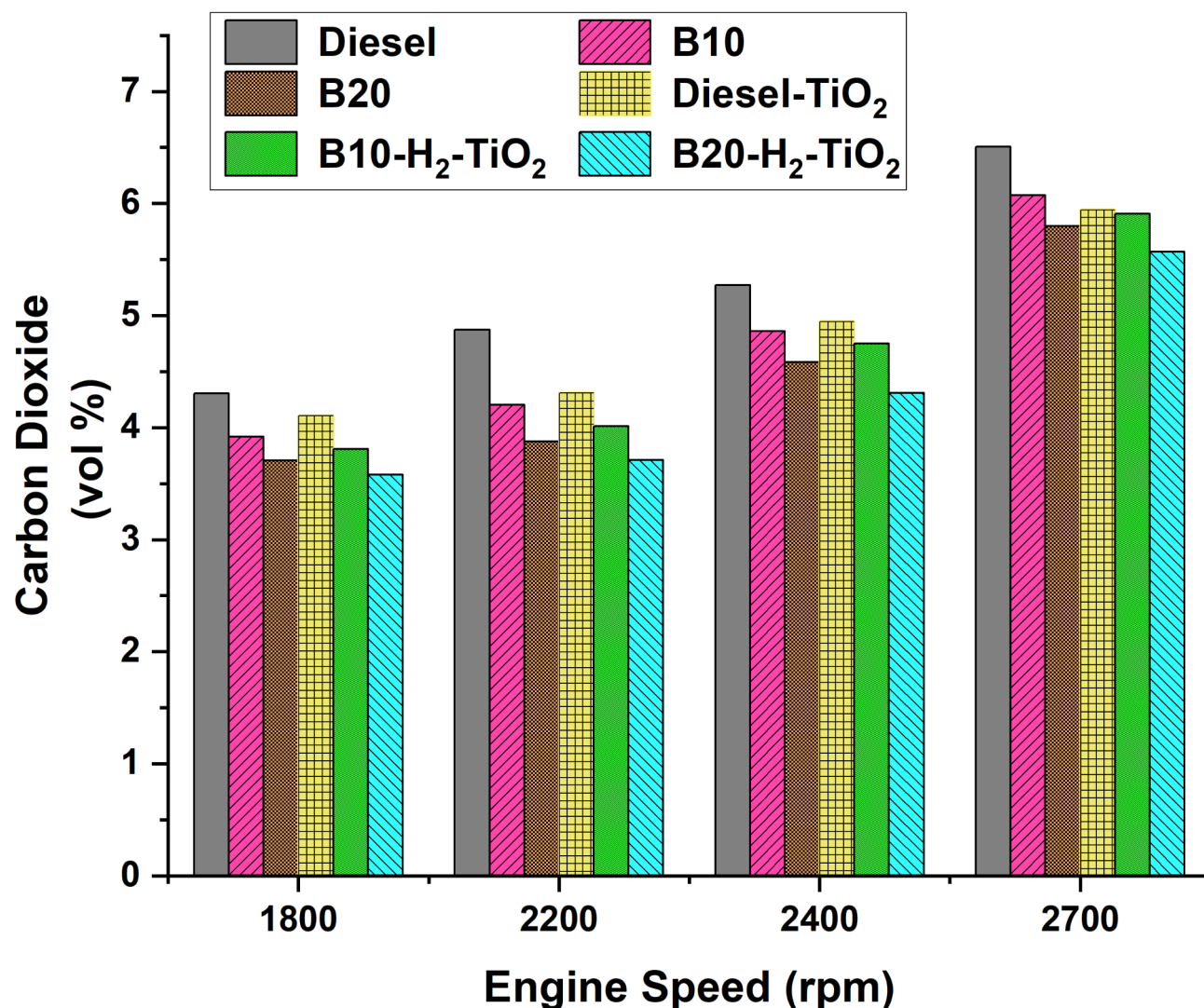


Fig. 19. Variation of carbon dioxide (CO₂) emission with respect to engine speed.

The MSRE, NSE and MAPE error standard measurements values for ANN tool optimized Diesel engine performance and pollutant emissions model was noticed in the range of (3.02 to 4.07% and 0.009057 to 0.008773). Then the overall correlation coefficient of the developed ANN network for the performance and pollutant emissions model were displayed from the Figs. 22, 23, 24, 25 and 26. In the Figs. 22 and 23, it was perceived that the ANN performance model (BTE and BSEC) results the R value in terms of training, validation, testing and all simulated value as (BTE) 0.99916, 0.99993, 0.99955 and 0.9993 and (BSEC) 0.99963, 0.99988, 0.99991 and 0.99969 correspondingly. Then Figs. 24, 25 and 26, it was noticed that the ANN emission model (CO, CO₂ and NO_x emission) yields the R value in terms of training, validation, testing and all simulated value as CO (0.993606, 0.99945, 0.9998 and 0.99838), CO₂ (0.99795, 0.99997, 0.99456 and 0.99725) and NO_x (0.9735, 1, 0.99847 and 0.98478).

Conclusion

This contemporary experimental investigation deals with biodiesel prepared with a novel immobilized lipase catalyst, and the present transesterification process was achieved. The collected GGME was analyzed with both physical and chemical properties, and it was correlated with ASTM and EURO fuel standards. The prepared GGME (biodiesel) achieved above 92% of biodiesel yield by eco-friendly lipase immobilized nanocatalyst which was tested with Kirloskar Diesel engine in terms of performance and tailpipe emissions and it results as follows: Diesel, B10, B20, Diesel-TiO₂, B10-H₂-TiO₂, and B20-H₂-TiO₂ were used for execution of all tests at varying engine speeds from 1800 rpm till 2700 rpm. The outcomes are provided below.

- The inclusion of nanoparticles and hydrogen improved the performance attributes, such as torque and brake thermal efficiency (BTE). In comparison with B10 (15.2%), the B10-H₂-TiO₂ has higher BTE (17%) which has an increase in BTE by about 11.84%. The primary cause of improved combustion resulting from inclusion

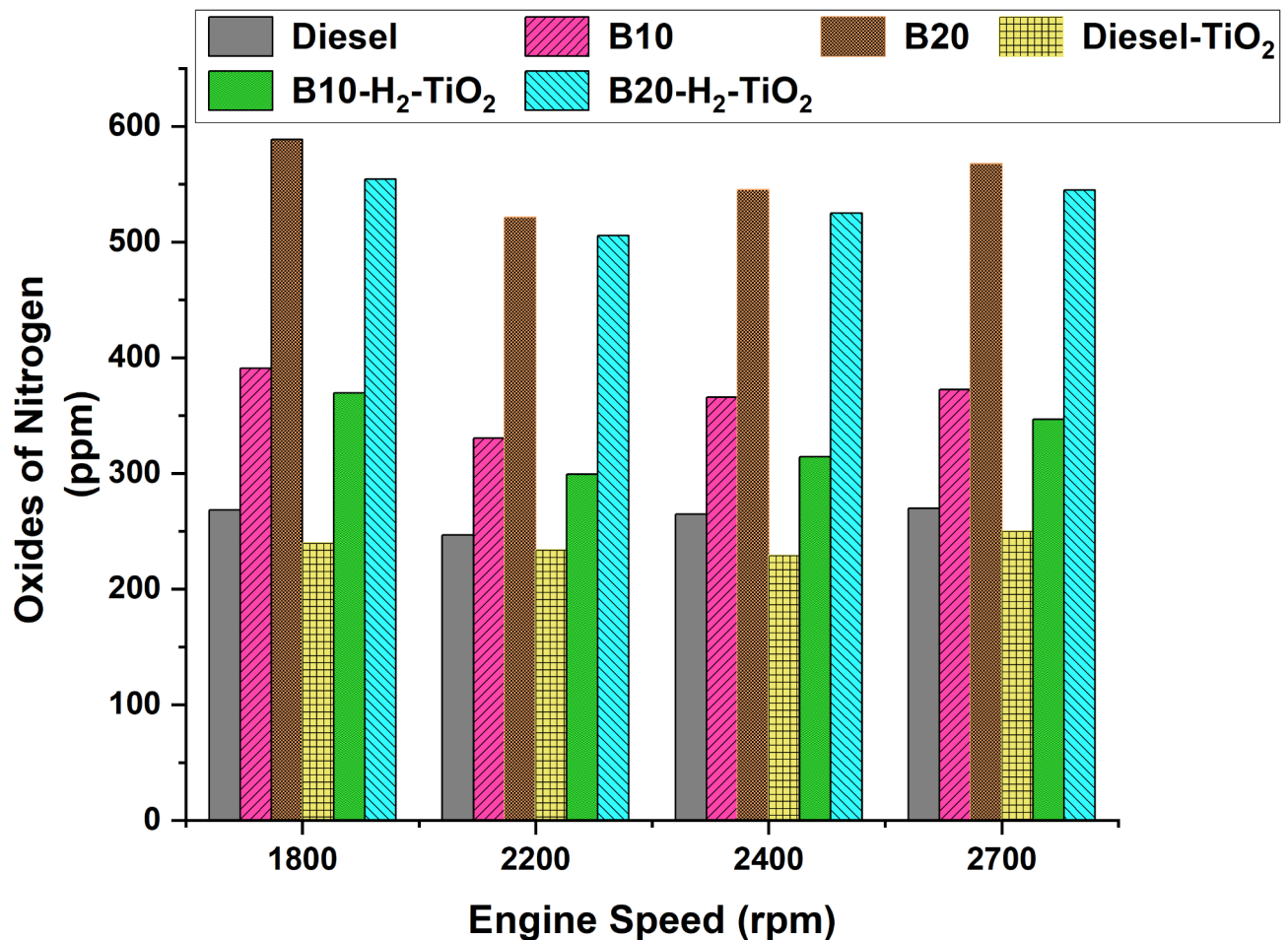


Fig. 20. Variation of oxides of nitrogen (NO_x) emission with respect to engine speed.

of H_2 gas (with higher flame velocity) and TiO_2 (improved diffusivity), followed by the lowered viscosity and higher oxygen content of the nanoparticle addition.

- When hydrogen and nanoparticles were added to fuel blends, the BSFC was likewise decreased. The enhanced fuel blends were not as high as fuel consumption of DIESEL, B10, and B20. Low specific fuel consumption can be attributed to improvement in combustion efficiency with addition of nano additives and hydrogen fuel which therefore contributes to higher fuel efficiency.
- It is evident from a comparison of the emission characteristics that enriched biofuel lowers the emissions of hazardous gases like CO and CO_2 . The decrease in CO and CO_2 rate is caused by complete combustion, which is achieved by the addition of hydrogen and nanoparticles, as well as charge dilution due to hydrogen results in overall lean combustion and carbon neutral characteristics. However, due of the elevated cylinder temperature, there was an increase in NO_x emissions. It is reasonable to say that adding hydrogen and nanoparticles improves the quality of the biodiesel overall. Higher NO_x emissions are environmental hazards but it can be mitigated by retarding the injection timing, water-in-emulsion, urea injection, etc.
- The proposed ANN model achieved accurate performance and pollutant model with optimal architecture, and the Diesel engine experimental data were precisely predicted and optimized. This ANN model was approved with the statistical error measurement values, namely relative mean square error, mean square relative error, Nash and Sutcliffe efficiency, an absolute fraction of variance, and mean fundamental percentage error. Moreover, the RSME had lowered rate of percentage error which was related with R value of the ANN model result.

Test fuel	Trail no	Brake power	Trail No	Brake power	Trail no	Brake power	Trail no	Brake power	Trail no	Brake power
Parameters	BTE		BSFC		NOx		CO		CO ₂	
B10	1.	0	2.	0	1.	0	1.	0	1.	0
B20	3.	0	4.	0	2.	0	2.	0	2.	0
Diesel-TiO ₂	5.	0	6.	0	3.	0	3.	0	3.	0
B10-H ₂ TiO ₂	7.	0	8.	0	4.	0	4.	0	4.	0
B20-H ₂ TiO ₂	9.	0	10.	0	5.	0	5.	0	5.	0
B10	11.	0	12.	0	6.	0	6.	0	6.	0
B20	13.	1.256	14.	1.256	7.	1.256	7.	1.256	7.	1.256
Diesel-TiO ₂	15.	1.256	16.	1.256	8.	1.256	8.	1.256	8.	1.256
B10-H ₂ TiO ₂	17.	1.256	18.	1.256	9.	1.256	9.	1.256	9.	1.256
B20-H ₂ TiO ₂	19.	1.256	20.	1.256	10.	1.256	10.	1.256	10.	1.256
B10	21.	1.256	22.	1.256	11.	1.256	11.	1.256	11.	1.256
B20	23.	1.256	24.	1.256	12.	1.256	12.	1.256	12.	1.256
Diesel-TiO ₂	25.	2.512	26.	2.512	13.	2.512	13.	2.512	13.	2.512
B10-H ₂ TiO ₂	27.	2.512	28.	2.512	14.	2.512	14.	2.512	14.	2.512
B20-H ₂ TiO ₂	29.	2.512	30.	2.512	15.	2.512	15.	2.512	15.	2.512
B10	31.	2.512	32.	2.512	16.	2.512	16.	2.512	16.	2.512
B20	33.	2.512	34.	2.512	17.	2.512	17.	2.512	17.	2.512
Diesel-TiO ₂	35.	2.512	36.	2.512	18.	2.512	18.	2.512	18.	2.512
B10-H ₂ TiO ₂	37.	3.768	38.	3.768	19.	3.768	19.	3.768	19.	3.768
B20-H ₂ TiO ₂	39.	3.768	40.	3.768	20.	3.768	20.	3.768	20.	3.768
B10	41.	3.768	42.	3.768	21.	3.768	21.	3.768	21.	3.768
B20	43.	3.768	44.	3.768	22.	3.768	22.	3.768	22.	3.768
Diesel-TiO ₂	45.	3.768	46.	3.768	23.	3.768	23.	3.768	23.	3.768
B10-H ₂ TiO ₂	47.	3.768	48.	3.768	24.	3.768	24.	3.768	24.	3.768
B20-H ₂ TiO ₂	49.	5.024	50.	5.024	25.	5.024	25.	5.024	25.	5.024
B10	51.	5.024	52.	5.024	26.	5.024	26.	5.024	26.	5.024
B20	53.	5.024	54.	5.024	27.	5.024	27.	5.024	27.	5.024
Diesel-TiO ₂	55.	5.024	56.	5.024	28.	5.024	28.	5.024	28.	5.024
B10-H ₂ TiO ₂	57.	5.024	58.	5.024	29.	5.024	29.	5.024	29.	5.024
B20-H ₂ TiO ₂	59.	5.024	60.	5.024	30.	5.024	30.	5.024	30.	5.024

Table 9. Design matrix output for various performance and emission parameters.

Engine characteristics	R ²	R	RMSE	MAPE
BSFC	0.99373	0.9996	0.250301	0.009057
BTE	0.992448	0.9993	0.419935	0.009585
CO	0.964267785	0.9983	0.002488626	0.025091
CO ₂	0.997672579	0.99725	0.031630703	0.006548
NO _x	0.984559489	0.9847	44.89075405	0.053824

Table 10. Error and performance of the ANN model.

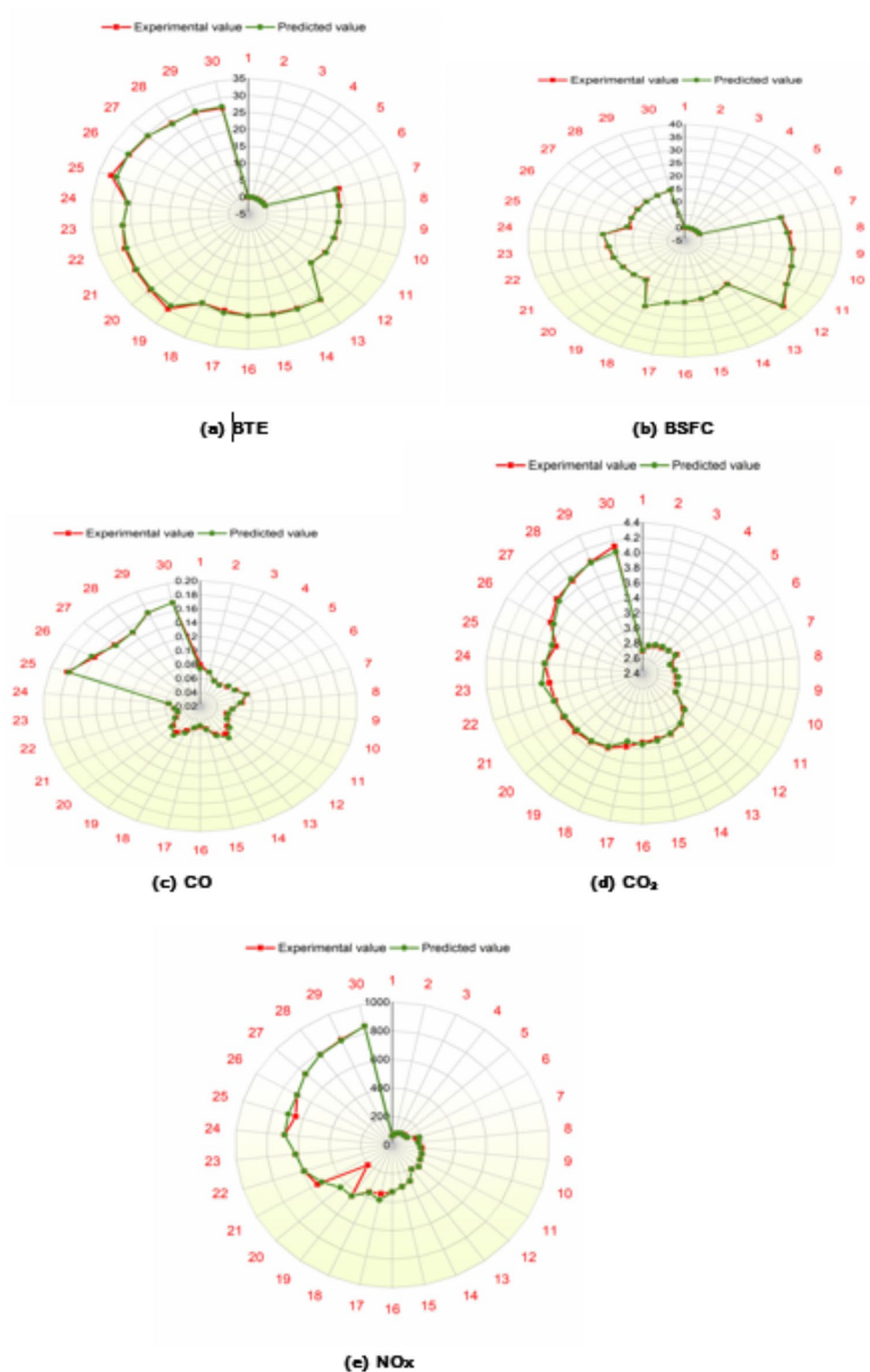


Fig. 21. Experimental and predicted results of (a) BTE (b) BSFC (c) CO (d) CO₂ and (e) NO_x.

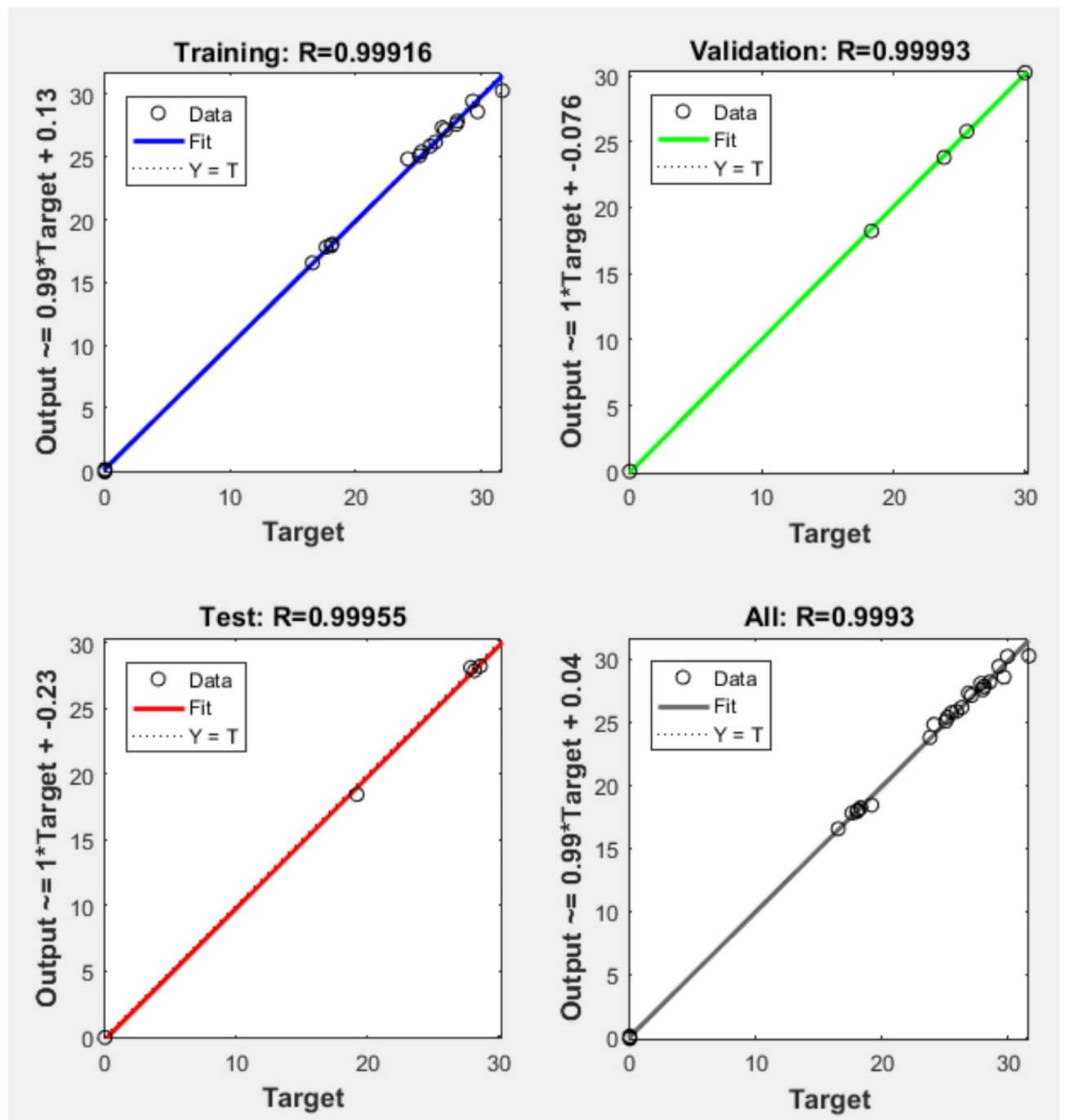


Fig. 22. Overall correlation coefficient and optimization of BTE.

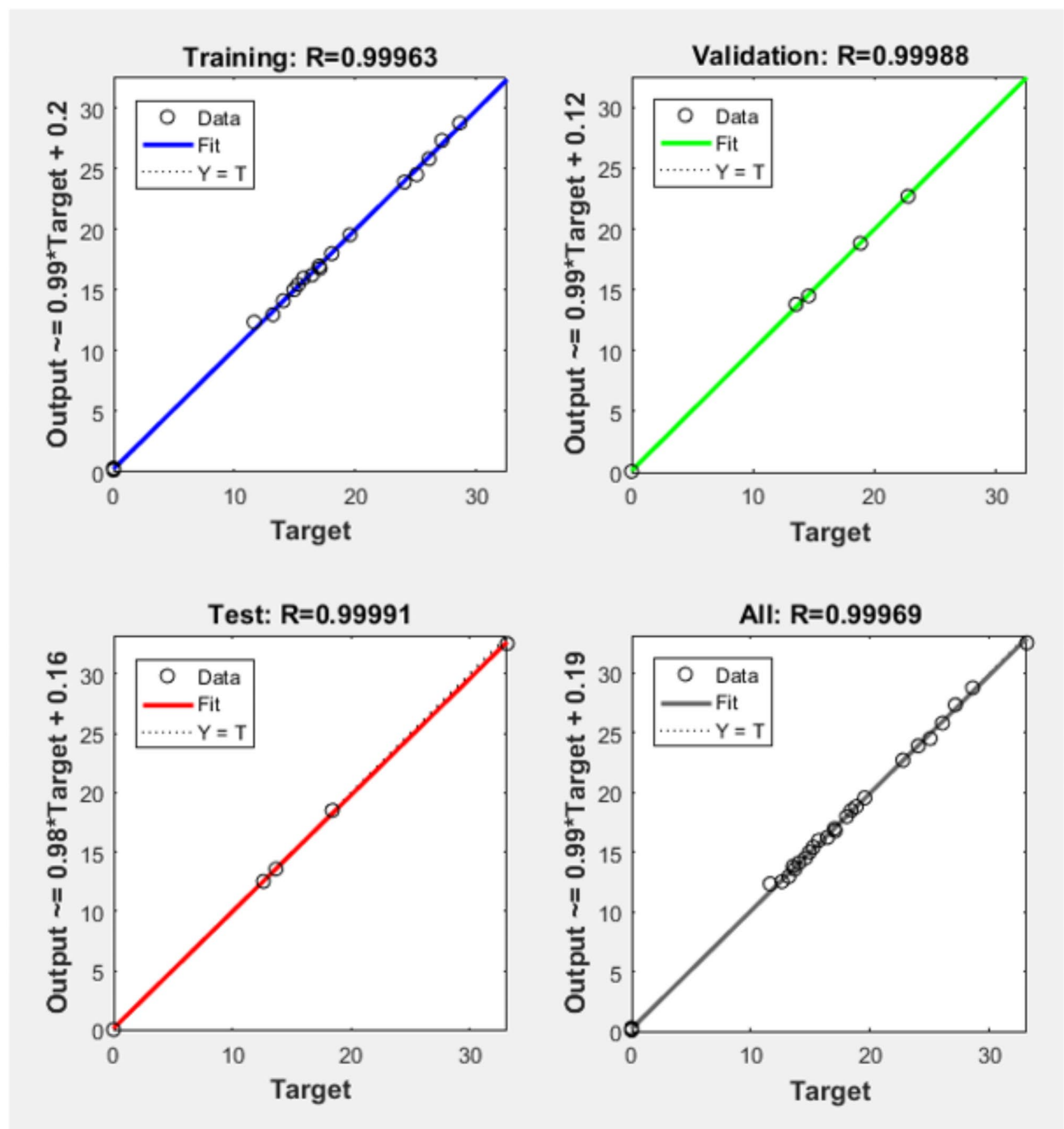


Fig. 23. Overall correlation coefficient and optimization of BSFC.

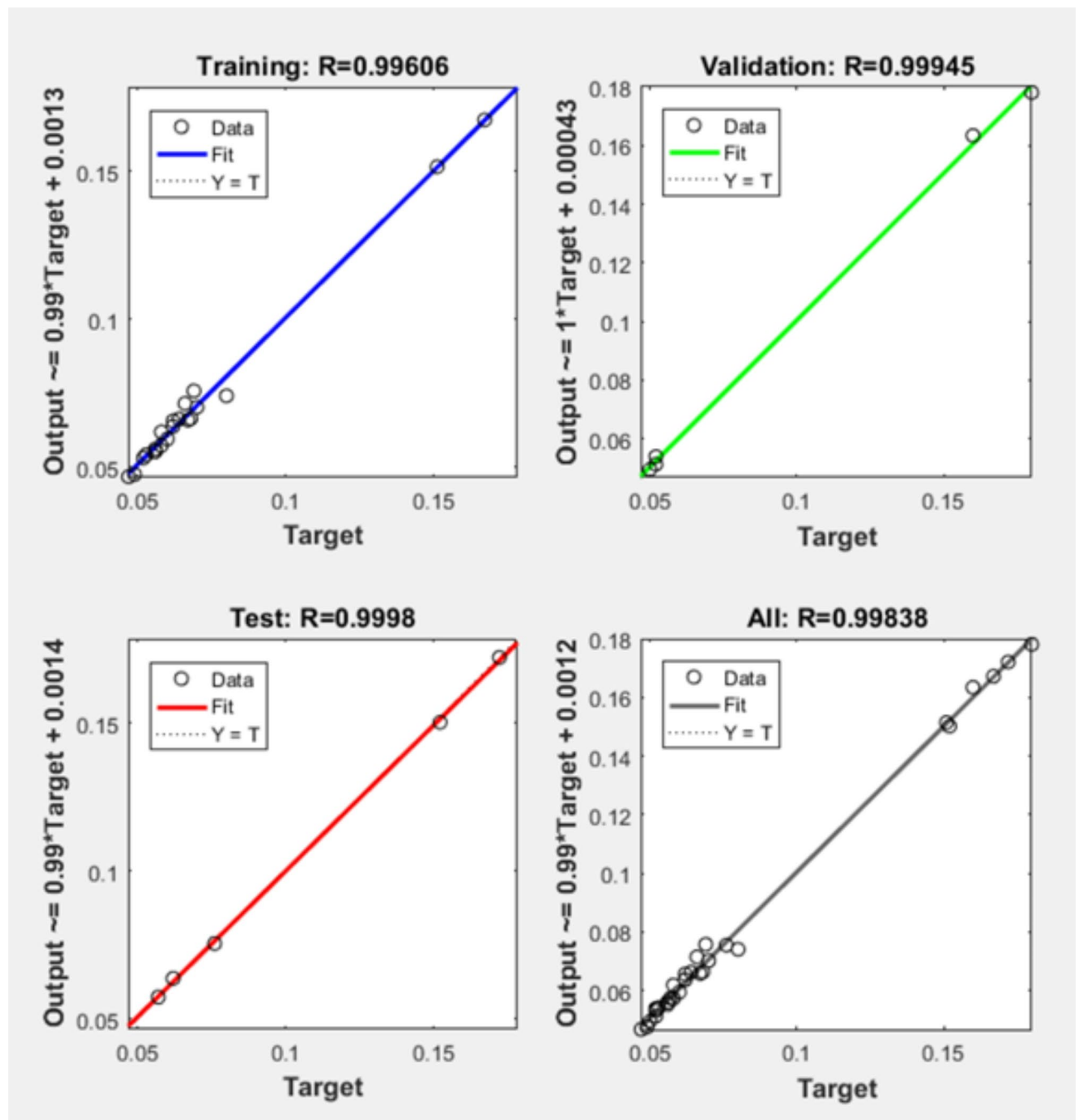


Fig. 24. Overall correlation coefficient and optimization of CO emission.

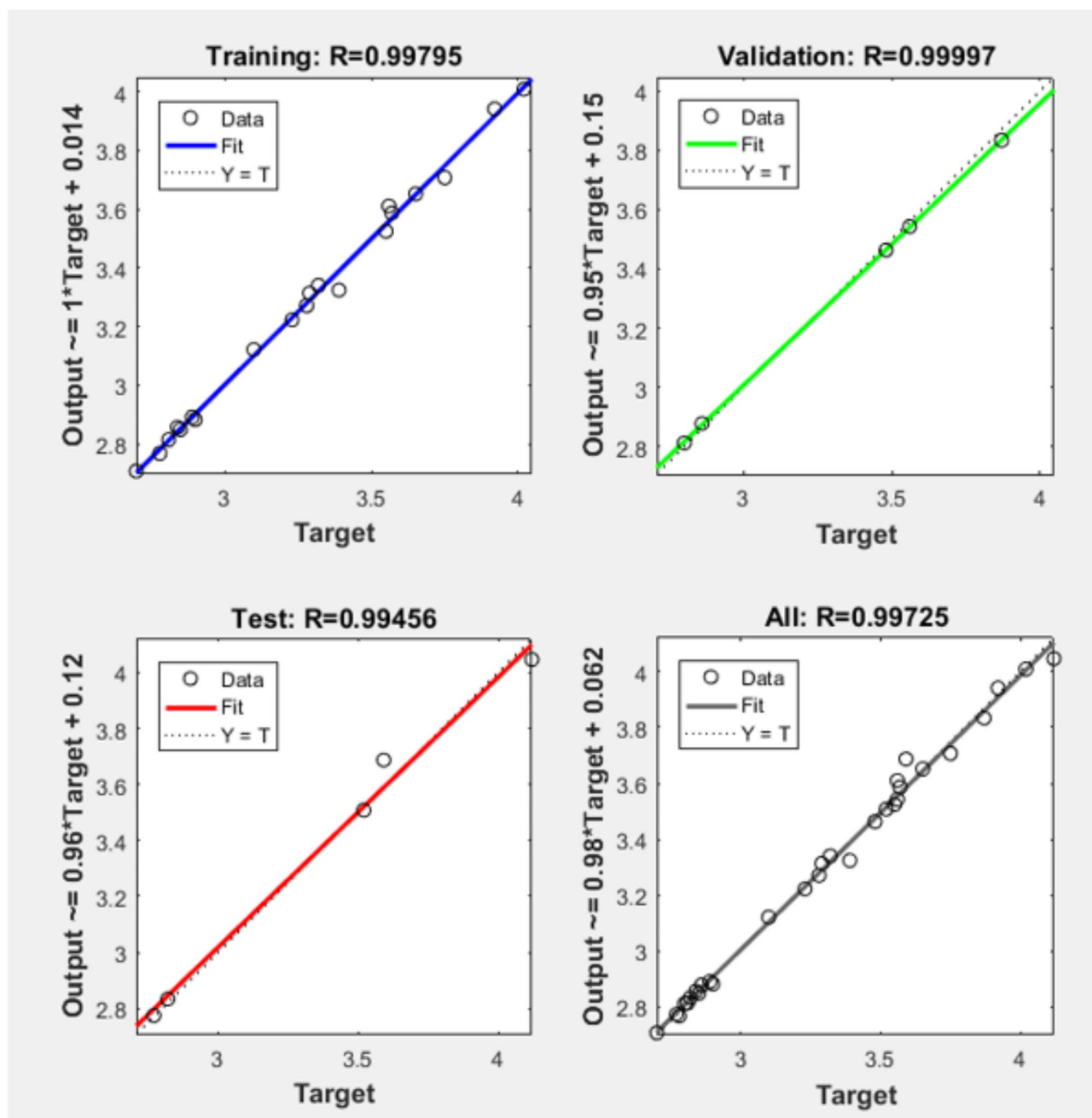


Fig. 25. Overall correlation coefficient and optimization of CO₂ emission.

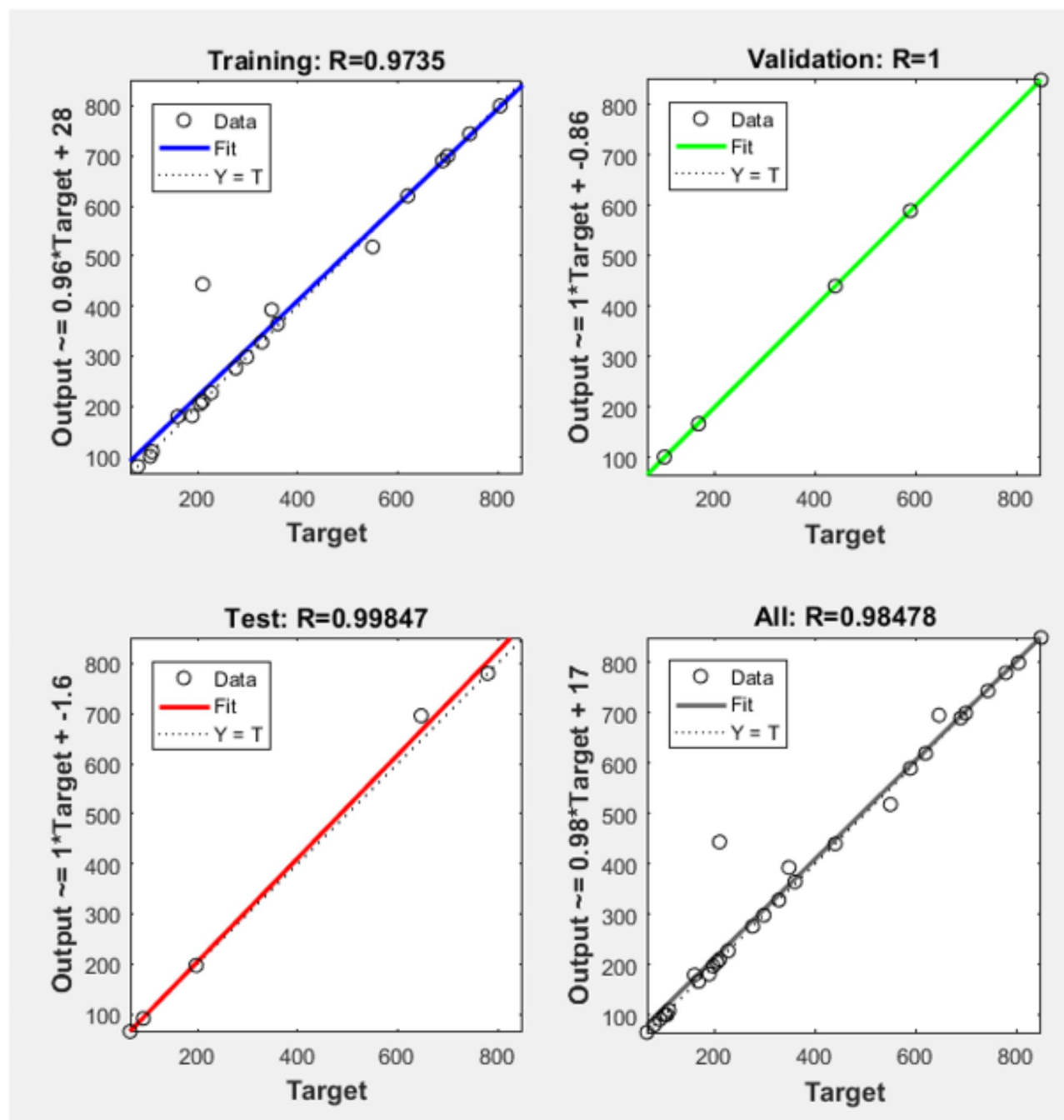


Fig. 26. Overall correlation coefficient and optimization of NOx emission.

Data availability

The datasets used and/or analysed during the current study available from the corresponding author on reasonable request.

Received: 25 July 2024; Accepted: 11 February 2025

Published online: 18 February 2025

References

1. Kumar, R. & Pal, P. Lipase immobilized graphene oxide biocatalyst assisted enzymatic transesterification of Pongamia pinnata (Karanja) oil and downstream enrichment of biodiesel by solar-driven direct contact membrane distillation followed by ultrafiltration. *Fuel Process. Technol.* **211**(June 2020), 106577. <https://doi.org/10.1016/j.fuproc.2020.106577> (2020).
2. Shalaeva, D. S. et al. Analysis of the development of global energy production and consumption by fuel type in various regions of the world. In *IOP Conference Series: Materials Science and Engineering*, vol. 952, No. 1, 012025. (IOP Publishing, 2020).

3. Ritchie, H., Rosado, P. & Roser, M. *Energy Production and Consumption*, Published online at OurWorldInData.org. <https://ourworldindata.org/energy-productionconsumption> (2020).
4. Subramanian, T., Geo, V. E. & Martin, L. J. Mitigation of carbon footprints through a blend of biofuels and oxygenates, combined with post-combustion capture system in a single cylinder CI engine. **130**. <https://doi.org/10.1016/j.renene.2018.07.010> (2019).
5. Kasiraman, G., Geo, V. E. & Nagalingam, B. Assessment of cashew nut shell oil as an alternate fuel for CI (Compression ignition) engines. *Energy*. **101**(x), 402–410. <https://doi.org/10.1016/j.energy.2016.01.086> (2016).
6. Khiari, K. et al. Experimental investigation of pistacia lentiscus biodiesel as a fuel for direct injection Diesel engine. *Energy. Convers. Manag.* **108**, 392–399. <https://doi.org/10.1016/j.enconman.2015.11.021> (2016).
7. Dharma, S. et al. Experimental study and prediction of the performance and exhaust emissions of mixed Jatropha curcas-Ceiba pentandra biodiesel blends in Diesel engine using artificial neural networks. *J. Clean. Prod.* **164**, 618–633. <https://doi.org/10.1016/j.jclepro.2017.06.065> (2017).
8. Javed, S., Satyanarayana Murthy, Y. V. V., Baig, R. U. & Prasada Rao, D. Development of ANN model for prediction of performance and emission characteristics of hydrogen dual fueled diesel engine with Jatropha Methyl Ester biodiesel blends. *J. Nat. Gas Sci. Eng.* **26**, 549–557. <https://doi.org/10.1016/j.jngse.2015.06.041> (2015).
9. Mohammadhassani, J., Dadvand, A., Khalilarya, S. & Solimanpur, M. Prediction and reduction of diesel engine emissions using a combined ANN-ACO method. *Appl. Soft Comput.* **34**, 139–150. <https://doi.org/10.1016/j.asoc.2015.04.059> (2015).
10. Ude, C. N. et al. Performance evaluation of cottonseed oil methyl esters produced using CaO and prediction with an artificial neural network. *Biofuels*. **7269**(July), 1–8. <https://doi.org/10.1080/17597269.2017.1345355> (2017).
11. Rajagopalachar, S., Joshi, S. S. & Reddy, R. P. Biodiesel synthesis from Garcinia gummi-gutta (L. Robson) seed oil : fuel feasibility evaluation of a novel feedstock by homogeneous and heterogeneous transesterification. *Biofuels* **0** (0), 1–8. <https://doi.org/10.1080/17597269.2017.1306681> (2017).
12. Ciftci, O. N. et al. Optimization of lipase production from organic solid waste by anaerobic digestion and its application in biodiesel production. *Energy. Conv. Manag.* **102** (1), 2130–2134. <https://doi.org/10.18331/BRJ2016.3.2.5> (2016).
13. Thiruvengadaravi, K. V. et al. Acid-catalyzed esterification of karanja (*Pongamia pinnata*) oil with high free fatty acids for biodiesel production. *Fuel* **98**, 1–4. <https://doi.org/10.1016/j.fuel.2012.02.047> (2012).
14. Sankaran, R. & Show, P. L. Biodiesel production using immobilized lipase: feasibility. <https://doi.org/10.1002/bbb> (2016).
15. Binhayeeding, N., Klomklao, S. & Prasertsan, P. Improvement of biodiesel production using waste cooking oil and applying single and mixed immobilised lipases on polyhydroxyalkanoate. *Renew. Energy*. **162**, 1819–1827. <https://doi.org/10.1016/j.renene.2020.10.009> (2020).
16. Hosseini, S. H., Taghizadeh-Alisaraei, A., Ghobadian, B. & Abbaszadeh-Mayvan, A. Performance and emission characteristics of a CI engine fuelled with carbon nanotubes and Diesel-biodiesel blends. *Renew. Energy*. **111**, 201–213. <https://doi.org/10.1016/j.renene.2017.04.013> (2017).
17. Betiku, E. et al. Mathematical modeling and process parameters optimization studies by artificial neural network and response surface methodology: a case of non-edible neem (*Azadirachta indica*) seed oil biodiesel synthesis. *Energy* **72**, 266–273. <https://doi.org/10.1016/j.energy.2014.05.033> (2014).
18. Rezaei, J., Shahbakhti, M., Bahri, B. & Aziz, A. A. Performance prediction of HCCI engines with oxygenated fuels using artificial neural networks. *Appl. Energy*. **138**, 460–473. <https://doi.org/10.1016/j.apenergy.2014.10.088> (2015).
19. Ilankumaran, M., Sakthivel, G. & Nagarajan, G. Artificial neural network approach to predict the engine performance of fish oil biodiesel with diethyl ether using back propagation algorithm. *Int. J. Ambient Energy*. **37** (5), 446–455. <https://doi.org/10.1080/01430750.2014.984082> (2016).
20. Subramani, L., Parthasarathy, M., Balasubramanian, D. & Ramalingam, K. Novel Garcinia gummi-gutta methyl ester (GGME) as a potential alternative feedstock for existing unmodified DI diesel engine. *Renew. Energy*. <https://doi.org/10.1016/j.renene.2018.02.134> (2018).
21. Amini, Z., Ilham, Z., Ong, H. C., Mazaheri, H. & Chen, W. H. State of the art and prospective of lipase-catalyzed transesterification reaction for biodiesel production. *Energy. Convers. Manag.* **141**, 339–353. <https://doi.org/10.1016/j.enconman.2016.09.049> (2017).
22. Karthickeyan, V., Balamurugan, P., Rohith, G. & Senthil, R. Developing of ANN model for prediction of performance and emission characteristics of VCR engine with orange oil biodiesel blends. *J. Braz. Soc. Mech. Sci. Eng.* **39** (7), 2877–2888. <https://doi.org/10.1007/s40430-017-0768-y> (2017).
23. Kannan, G. R., Karvembu, R. & Anand, R. Effect of metal based additive on performance emission and combustion characteristics of diesel engine fuelled with biodiesel. **88**, 3694–3703. <https://doi.org/10.1016/j.apenergy.2011.04.043> (2011).
24. Kakati, J. & Gogoi, T. K. Biodiesel production from Kutkura (Meyna Spinosa Roxb. Ex.) Fruit seed oil: its characterization and engine performance evaluation with 10% and 20% blends. *Energy. Convers. Manag.* **121**, 152–161. <https://doi.org/10.1016/j.enconman.2016.05.019> (2016).
25. Alagu, K. et al. Novel water hyacinth biodiesel as a potential alternative fuel for existing unmodified Diesel engine: performance, combustion and emission characteristics. *Energy* **179**, 295–305. <https://doi.org/10.1016/j.energy.2019.04.207> (2019).
26. Silitonga, A. S., Masjuki, H. H., Mahlia, T. M. I., Ong, H. C. & Chong, W. T. Experimental study on performance and exhaust emissions of a Diesel engine fuelled with Ceiba pentandra biodiesel blends. *Energy. Convers. Manag.* **76**, 828–836. <https://doi.org/10.1016/j.enconman.2013.08.032> (2013).
27. Pourvosoughi, N. et al. Polysel: an environmental-friendly CI engine fuel. *Energy* **111**, 691–700. <https://doi.org/10.1016/j.energy.2016.05.125> (2016).
28. Kumar, N. & Ram, S. Performance and emission characteristics of biodiesel from different origins: a review. *Renew. Sustain. Energy Rev.* **21**, 633–658. <https://doi.org/10.1016/j.rser.2013.01.006> (2013).
29. Venu, H. An experimental assessment on the influence of fuel-borne additives on ternary fuel (Diesel–biodiesel–ethanol) blends operated in a single cylinder Diesel engine. *Environ. Sci. Pollut. Res.* **2014** <https://doi.org/10.1007/s11356-019-04739-5> (2019).
30. Sharma, A. & Murugan, S. Combustion, performance and emission characteristics of a di Diesel engine fuelled with non-petroleum fuel: a study on the role of fuel injection timing. *J. Energy Inst.* **88** (4), 364–375. <https://doi.org/10.1016/j.joei.2014.11.006> (2015).
31. Nair, J. N., Kaviti, A. K. & Daram, A. K. Analysis of performance and emission on compression ignition engine fuelled with blends of neem biodiesel. *Egypt. J. Pet.* **26** (4), 927–931. <https://doi.org/10.1016/j.ejpe.2016.09.005> (2017).
32. Lingesan, S. et al. Production of Garcinia gummi-gutta methyl ester (GGME) as a potential alternative feedstock for existing unmodified DI Diesel Engine: Combustion, Performance, and Emission characteristics. *J. Test. Eval.* **46** (6), 20170246. <https://doi.org/10.1520/jte20170246> (2018).
33. Ghareghani, A., Mirsalim, M. & Hosseini, R. Effects of waste fish oil biodiesel on Diesel engine combustion characteristics and emission. *Renew. Energy*. **101**, 930–936. <https://doi.org/10.1016/j.renene.2016.09.045> (2017).
34. Shahir, S. A., Masjuki, H. H., Kalam, M. A., Imran, A. & Ashraf, A. M. Performance and emission assessment of diesel–biodiesel–ethanol/bioethanol blend as a fuel in Diesel engines: a review. *Renew. Sustain. Energy Rev.* **48**, 62–78. <https://doi.org/10.1016/j.rser.2015.03.049> (2015).
35. Lotfan, S., Ghiasi, R. A., Fallah, M. & Sadeghi, M. H. ANN-based modeling and reducing dual-fuel engine's challenging emissions by multi-objective evolutionary algorithm NSGA-II. *Appl. Energy*. **175**, 91–99. <https://doi.org/10.1016/j.apenergy.2016.04.099> (2016).
36. Ramalingam, K. et al. An assessment of combustion, performance characteristics and emission control strategy by adding anti-oxidant additive in emulsified fuel. *Atmos. Pollut. Res.* 1–0. <https://doi.org/10.1016/j.apr.2018.02.007> (2018).

37. Ganesan, P., Rajakarunakaran, S., Thirugnanasambandam, M. & Devaraj, D. Artificial neural network model to predict the diesel electric generator performance and exhaust emissions. *Energy* **83**, 115–124. <https://doi.org/10.1016/j.energy.2015.02.094> (2015).
38. Channappattana, S. V., Pawar, A. A. & Kamble, P. G. Optimisation of operating parameters of DI-CI engine fuelled with second generation bio-fuel and development of ANN based prediction model. *Appl. Energy*. **187**, 84–95. <https://doi.org/10.1016/j.apenergy.2016.11.030> (2017).
39. Betiku, E. et al. Predictive capability evaluation of RSM, ANFIS and ANN: a case of reduction of high free fatty acid of palm kernel oil via esterification process. *Energy. Conv. Manag.* **124**, 219–230. <https://doi.org/10.1016/j.enconman.2016.07.030> (2016).
40. Deb, M., Majumder, P., Majumder, A., Roy, S. & Banerjee, R. Application of artificial intelligence (AI) in characterization of the performance–emission profile of a single cylinder CI engine operating with hydrogen in dual fuel mode: an ANN approach with fuzzy-logic based topology optimization. *Int. J. Hydrog. Energy*. **41** (32), 14330–14350 (2016).
41. Liu, J., Duan, X., Yuan, Z., Liu, Q. & Tang, Q. Experimental study on the performance, combustion and emission characteristics of a high compression ratio heavy-duty spark-ignition engine fuelled with liquefied methane gas and hydrogen blend. *Appl. Therm. Eng.* **124**, 585–594 (2017).
42. Alrazen, H. A., Talib, A. A., Adnan, R. & Ahmad, K. A. A review of the effect of hydrogen addition on the performance and emissions of the compression–ignition engine. *Renew. Sustain. Energy Rev.* **54**, 785–796 (2016).
43. Luo, J. et al. Investigation of hydrogen addition on the combustion, performance, and emission characteristics of a heavy-duty engine fuelled with diesel/natural gas. *Energy*. **260**, 125082 (2022).
44. Zhou, J. H., Cheung, C. S. & Leung, C. W. Combustion, performance, regulated and unregulated emissions of a diesel engine with hydrogen addition. *Appl. Energy*. **126**, 1–12 (2014).
45. Hedayat, F. et al. Influence of oxygen content of the certain types of biodiesels on particulate oxidative potential. *Sci. Total Environ.* **545**, 381–388 (2016).
46. Randazzo, M. L. & Sodré, J. R. Exhaust emissions from a Diesel powered vehicle fuelled by soybean biodiesel blends (B3–B20) with ethanol as an additive (B20E2–B20E5). *Fuel* **90** (1), 98–103 (2011).
47. Luo, Q. H. et al. Experimental investigation of combustion characteristics and NOx emission of a turbocharged hydrogen internal combustion engine. *Int. J. Hydrog. Energy*. **44** (11), 5573–5584 (2019).
48. Li, J., Huang, H., Kobayashi, N., He, Z. & Nagai, Y. Study on using hydrogen and ammonia as fuels: Combustion characteristics and NOx formation. *Int. J. Energy Res.* **38** (9), 1214–1223 (2014).
49. Shin, B., Cho, Y., Han, D., Song, S. & Chun, K. M. Hydrogen effects on NOx emissions and brake thermal efficiency in a Diesel engine under low-temperature and heavy-EGR conditions. *Int. J. Hydrog. Energy*. **36** (10), 6281–6291 (2011).
50. Subramani, L., Annamalai, K., Parthasarathy, M., Lalvani, I. J. R. & Moorthy, K. Production of Garcinia gummi-gutta methyl ester (GGME) as a potential alternative feedstock for existing unmodified DI diesel engine: combustion, performance and emission characteristics. *J. Test. Eval.* **1** (1). (2018).
51. Venu, H., Subramani, L. & Raju, V. D. Emission reduction in a DI diesel engine using exhaust gas recirculation (EGR) of palm biodiesel blended with TiO₂ nano additives. *Renew. Energy*. **140**, 245–263 (2019).
52. Subramani, L., Parthasarathy, M., Balasubramanian, D. & Ramalingam, K. Novel Garcinia gummi-gutta methyl ester (GGME) as a potential alternative feedstock for existing unmodified DI diesel engine. *Renew. Energy*. **125**, 568–577 (2018).
53. Venu, H. et al. A comprehensive combustion, performance, and environmental analyses of algae biofuel, hydrogen gas, and nano-sized particles (liquid-gas-solid mix) in agricultural CRDI engines. *Int. J. Hydrog. Energy*. **73**, 839–855 (2024).
54. Attia, A. M., El-Seesy, A. I., El-Batsh, H. M. & Shehata, M. S. Effects of alumina nanoparticles additives into Jojoba methyl ester-diesel mixture on diesel engine performance. In *ASME International Mechanical Engineering Congress and Exposition*, vol. 46521, V06BT07A019 (2014).
55. Arockiasamy, P. & Anand, R. B. Performance, combustion and emission characteristics of a DI diesel engine fuelled with nanoparticle blended jatropha biodiesel. *Periodica Polytechnica Mech. Eng.* **59** (2), 88–93 (2015).
56. Aalam, C. S., Saravanan, C. G. & Kannan, M. Experimental investigations on a CRDI system assisted diesel engine fuelled with aluminium oxide nanoparticles blended biodiesel. *Alexandria Eng. J.* **54** (3), 351–358 (2015).
57. Shaafi, T. & Velraj, R. Influence of alumina nanoparticles, ethanol and isopropanol blend as additive with diesel–soybean biodiesel blend fuel: Combustion, engine performance and emissions. *Renew. Energy*. **80**, 655–663 (2015).
58. Anbarasu, A., Karthikeyan, A. & Balaji, M. Performance and emission characteristics of diesel engine using alumina nanoparticle blended biodiesel emulsion fuel. *J. Energy Res. Technol.* **138** (2), 022203–022201 (2016).
59. Prabu, A. & Anand, R. B. Emission control strategy by adding alumina and cerium oxide nanoparticle in biodiesel. *J. Energy Inst.* **89** (3), 366–372 (2016).
60. Sharma, S. K., Das, R. K. & Sharma, A. Improvement in the performance and emission characteristics of diesel engine fuelled with jatropha methyl ester and tyre pyrolysis oil by addition of nano additives. *J. Braz. Soc. Mech. Sci. Eng.* **38**(7), 1907–1920 (2015).
61. Patel, H. K. & Kumar, S. Experimental analysis on performance of diesel engine using mixture of diesel and bio-diesel as a working fuel with aluminum oxide nanoparticle additive. *Therm. Sci. Eng. Progr.* **4**, 252–258 (2017).
62. Sivakumar, M., Sundaram, N. S. & Thasthagir, M. H. S. Effect of aluminium oxide nanoparticles blended pongamia methyl ester on performance, combustion and emission characteristics of diesel engine. *Renew. Energy*. **116**, 518–526 (2018).
63. Hosseini, S. H., Taghizadeh-Alisaraei, A., Ghobadian, B. & Abbaszadeh-Mayvan, A. Effect of added alumina as nano-catalyst to diesel-biodiesel blends on performance and emission characteristics of CI engine. *Energy*. **124**, 543–552 (2017).
64. Gumus, S., Ozcan, H., Ozbey, M. & Topaloglu, B. Aluminum oxide and copper oxide nanodiesel fuel properties and usage in a compression ignition engine. *Fuel* **163**, 80–87 (2016).
65. Chandrasekaran, V., Arthanarisamy, M., Nachiappan, P., Dhanakotti, S. & Moorthy, B. The role of nano additives for biodiesel and diesel blended transportation fuels. *Transport. Res. Part D. Transp. Environ.* **46**, 145–156 (2016).
66. Kannan, G. R., Karvembu, R. & Anand, R. Effect of metal based additive on performance emission and combustion characteristics of diesel engine fuelled with biodiesel. *Appl. Energy*. **88**(11), 3694–3703 (2011).
67. Mohan, B., Yang, W., Raman, V., Sivasankaralingam, V. & Chou, S. K. Optimisation of biodiesel fueled engine to meet emission standards through varying nozzle opening pressure and static injection timing. *Appl. Energy*. **130**, 450–457 (2014).
68. Sivakumar, M., Sundaram, N. S. & Thasthagir, M. H. S. Effect of aluminium oxide nanoparticles blended pongamia methyl ester on performance, combustion and emission characteristics of diesel engine. *Renew. Energy*. **116**, 518–526 (2018).
69. Ranjan, A. et al. Experimental investigation on effect of MgO nanoparticles on cold flow properties, performance, emission and combustion characteristics of waste cooking oil biodiesel. *Fuel* **220**, 780–791 (2018).
70. Mehregan, M. & Moghiman, M. Effects of nano-additives on pollutants emission and engine performance in a urea-SCR equipped diesel engine fuelled with blended-biodiesel. *Fuel* **222**, 402–406 (2018).
71. El-Seesy, A. I., Attia, A. M. & El-Batsh, H. M. The effect of aluminum oxide nanoparticles addition with Jojoba methyl ester-diesel fuel blend on a diesel engine performance, combustion and emission characteristics. *Fuel* **224**, 147–166 (2018).
72. Hoseini, S. S. et al. Novel environmentally friendly fuel: the effects of nanographene oxide additives on the performance and emission characteristics of diesel engines fuelled with Ailanthus altissima biodiesel. *Renew. Energy*. **125**, 283–294 (2018).
73. Kumar, S., Dinesha, P. & Bran, I. Influence of nanoparticles on the performance and emission characteristics of a biodiesel fuelled engine: an experimental analysis. *Energy* **140**, 98–105 (2017).
74. Ashok, B., Nanthagopal, K., Mohan, A., Johny, A. & Tamilarasu, A. Comparative analysis on the effect of zinc oxide and ethanox as additives with biodiesel in CI engine. *Energy* **140**, 352–364 (2017).

75. Leo, G. L. et al. Predicting the performance and emissions of an HCCI-DI engine powered by waste cooking oil biodiesel with Al_2O_3 and FeCl_3 nano additives and gasoline injection—A random forest machine learning approach. *Fuel* **357**, 129914 (2024).
76. Mohanrajhu, N., Sekar, S., Jayabal, R. & Sureshkumar, R. Screening nano additives for favorable NO_x /smoke emissions trade-off in a CRDI diesel engine fueled by industry leather waste fat biodiesel blend. *Process Saf. Environ. Prot.* **187**, 332–342 (2024).
77. Jayabal, R. et al. Study of the effects of bio-silica nanoparticle additives on the performance, combustion, and emission characteristics of biodiesel produced from waste fat. *Sci. Rep.* **13** (1), 18907 (2023).

Acknowledgements

The authors wish to acknowledge the financial support provided by AAIBE Chair of Renewable Energy at UNIT-EN (grant no: 201801KETTHA).

The authors also extend their appreciation to the Deanship of Scientific Research at King Khalid University, Abha, Kingdom of Saudi Arabia for funding this work through Large Groups R.G.P. 2/127/45.

Author contributions

Conceptualization-H.V., T.S.K.; Investigation-H.V. and N.M.R.; Methodology-M.A.K.; Supervision, validation-T.S.K.; Writing—original draft, H.V., M.E.M.S. and N.M.R.; Review and editing-M.E.M.S., E.C., H.-R.W., and N.A. Funding acquisition T.M.Y.K.

Declarations

Competing interests

The authors declare no competing interests.

Additional information

Correspondence and requests for materials should be addressed to M.E.M.S. or E.C.

Reprints and permissions information is available at www.nature.com/reprints.

Publisher's note Springer Nature remains neutral with regard to jurisdictional claims in published maps and institutional affiliations.

Open Access This article is licensed under a Creative Commons Attribution-NonCommercial-NoDerivatives 4.0 International License, which permits any non-commercial use, sharing, distribution and reproduction in any medium or format, as long as you give appropriate credit to the original author(s) and the source, provide a link to the Creative Commons licence, and indicate if you modified the licensed material. You do not have permission under this licence to share adapted material derived from this article or parts of it. The images or other third party material in this article are included in the article's Creative Commons licence, unless indicated otherwise in a credit line to the material. If material is not included in the article's Creative Commons licence and your intended use is not permitted by statutory regulation or exceeds the permitted use, you will need to obtain permission directly from the copyright holder. To view a copy of this licence, visit <http://creativecommons.org/licenses/by-nc-nd/4.0/>.

© The Author(s) 2025